

Research Article

Indigo Carmine and 2,6-Dichlorophenolindophenol Removal Using Cetyltrimethylammonium Bromide-Modified Palm Oil Fiber: Adsorption Isotherms and Mass Transfer Kinetics

Marcel Cédric Deussi Ngaha, Evangéline Njanja , Giscard Doungmo, Arnaud Tamo Kamdem, and Ignas Kenfack Tonle 

Electrochemistry and Chemistry of Materials, Department of Chemistry, Faculty of Science, University of Dschang, P.O. Box 67, Dschang, Cameroon

Correspondence should be addressed to Evangéline Njanja; njanja.tcheunkeu@univ-dschang.org

Received 29 June 2019; Accepted 5 November 2019; Published 13 December 2019

Academic Editor: Wen-Cheng Chen

Copyright © 2019 Marcel Cédric Deussi Ngaha et al. This is an open access article distributed under the Creative Commons Attribution License, which permits unrestricted use, distribution, and reproduction in any medium, provided the original work is properly cited.

In the present work, the usefulness of cetyltrimethylammonium bromide-modified palm oil fiber (CTAB-modified POF) for the removal of indigo carmine (IC) and 2,6-dichlorophenolindophenol (2,6-DCPIP) from aqueous solutions was investigated. Raw, NaOH-treated, and CTAB-modified POF were characterized by Fourier-transform infrared (FT-IR) spectroscopy, elemental analysis, thermogravimetric-hyperdifferential scanning calorimetric (TG-HDSC) analysis, X-ray diffraction (XRD), and scanning electron microscopy (SEM). The adsorption studies of IC and 2,6-DCPIP were performed in batch mode using CTAB-modified POF. The results showed that equilibrium was attained after a contact time of 30 minutes for IC and 20 minutes for 2,6-DCPIP. The maximum capacity of adsorption was obtained at pH = 2. The capacity of adsorption considerably increased with modified biosorbents and with increasing initial concentration of dyes. The ionic strength favors the increasing adsorption capacity of IC and does not affect the adsorption capacity of 2,6-DCPIP. The percentage of adsorption increased with increasing mass of the biosorbents. The nonlinear regression of adsorption isotherms showed that Freundlich ($r^2 = 0.953$; $\chi^2 = 4.398$) and Temkin ($r^2 = 0.986$; $\chi^2 = 1.196$) isotherms are most appropriate to describe the adsorption of IC and 2,6-DCPIP on CTAB-modified POF, respectively. The maximum adsorption capacities determined by the Langmuir isotherm were 275.426 and 230.423 $\mu\text{mol}\cdot\text{g}^{-1}$ for IC and 2,6-DCPIP, respectively. The linear regression of adsorption kinetics was best described by the pseudo-second-order model ($R^2 \geq 0.998$). The diffusion mechanism showed that external mass transfer is the main rate controlling step. Desorption of the two dyes is favorable in the alkaline medium.

1. Introduction

Most dyes are organic compounds having complex aromatic structures with a variety of functional groups and are extensively used in various industries like textile, paper, plastic, food, printing, cosmetic, and pharmaceutical industries [1–3]. However, some dyes discharged from the effluents of the industries into receiving streams are sources of water pollution because most of the dyes and their degradation products are highly toxic, mutagenic, carcinogenic, and allergenic [4–7]. The dyes in water effluents have a very hazardous impact on the environment, making it unfit for

human and aquatic life, thus causing chronic and acute diseases [3–8]. Therefore, several treatment methods have been adopted for removal of dyes from wastewaters in view to prevent continuous environmental pollution.

The traditional methods used for removing dyes from wastewaters include flocculation, electroflotation, chemical precipitation, electrokinetic coagulation, ion exchange, membrane filtration, electrochemical destruction, irradiation, ozonation, and microbial biodegradation [9, 10]. However, application of these methods is restricted because they are ineffective and noneconomical and have many disadvantages such as high reagent and energy

requirements, generation of toxic sludge, or other waste products that require disposal or treatment [6, 11]. The adsorption technique is the most used in industries for advanced wastewater treatment because it is efficient, simple to design, and does not produce any sludge [1, 12, 13]. The commercial activated carbon has been the first adsorbent used in adsorption. Because of high cost of activated carbon and problems of regeneration of adsorbents after adsorption [14], several research studies were conducted to the use of new adsorbents that are lower in cost, locally available, and efficient [3, 12]: they are lignocellulosic materials. Ever since, adsorption of some dyes on many lignocellulosic materials such as rice husk, orange peel, coconut husk, barley husks, peanut hull, eggshell, cocoa shell [13], hazelnut shells [15], olive stone [16], sugarcane bagasse [17], palm tree trunk [3], and wood sawdust [18] have been investigated, and all of these are effective for dyes removal. However, the modification of these lignocellulosic materials also seems necessary to improve their performance. Some earlier works mentioned that the modification of biosorbents with cationic surfactants is an effective technology to enhance the adsorption capacity of anionic dyes [7, 19–22].

The aim of our work is to valorize the palm grove residues for the biosorption of some organic dyes. In our previous work, we investigate about a natural- and acetic acid-treated palm tree trunk for the adsorption of 2,6-DCPIP [3]. The present study aims to evaluate the potentialities of palm oil fiber modified with cationic surfactants, such as cetyltrimethylammonium bromide, in order to enhance the adsorption capacity towards IC and 2,6-DCPIP from aqueous solutions. The effects of some important parameters such as modification of biosorbents, initial dye concentration, pH of solutions, adsorbent dosage, ionic strength, and contact time on the adsorption of both IC and 2,6-DCPIP onto CTAB-modified POF were compared. The adsorption was described by using adsorption isotherms and kinetic models. The possibility of dyes recovering and to reuse the biosorbent was also investigated.

2. Materials and Methods

2.1. Materials, Preparations, and Characterizations of Biomass. All chemical reagents used in this experiment were obtained commercially and used without further purification. NaCl and NaOH were purchased from Fisher, IC dye content 85% was purchased from Sigma-Aldrich, HCl was purchased from Phillip Harris, AgNO₃ was purchased from Kem Light, HNO₃ and 2,6-DCPIP were purchased from Riedel-de-Häen, and CTAB was purchased from Prolabo.

The palm oil fiber used in this work was kindly provided by a local palm oil producer in the Littoral region of Cameroon. The material was cleaned, cut into small pieces, washed several times with tap water to remove impurities such as sand, dust, and soil particles, and then dried for 8 days in sunlight. The dried biomass was ground into fine powder and sieved to obtain sizes lower than 100 μm for further analyses.

Prior to the modification with CTAB, the raw POF was first submitted to pretreatment with NaOH solution, according to the following procedure: 5 g of raw POF was stirred on a mechanical platform shaker (Edmund Bühler GmbH) in 100 mL of 2 mol·L⁻¹ NaOH solution for 2 h at a speed of 200 rpm. The obtained material was washed several times with distilled water (in order to remove the excess of NaOH until the neutral pH of washed water was measured), air-dried for 2 days, and then placed in an oven at 110°C for 24 h before use.

For the modification with CTAB, 1 g of NaOH-treated POF freshly removed from the oven was dispersed in 100 mL of 14 mmol·L⁻¹ CTAB solution. The whole was also agitated on a mechanical platform shaker (Edmund Bühler GmbH) for a time period of 24 h at a speed of 200 rpm. Afterwards, the suspension was filtered, and the resultant material was washed several times with distilled water for the removal of superficially retained CTAB until no white precipitate was formed on addition of AgNO₃ (0.1 mol·L⁻¹) to the washed water. The obtained biosorbent was dried in an oven at 60°C for 24 h before being sieved and kept in a bottle for further use.

The raw, NaOH-treated, and CTAB-modified POF were characterized using Fourier-transform infrared spectroscopy, elemental analysis, thermogravimetric-hyperdifferential scanning calorimetric analysis, X-ray diffraction analysis, and scanning electron microscopy. The FT-IR spectra were obtained by means of the ATR technique with a FT-IR spectrophotometer (Bruker α-P, Germany) within a range of 4000–400 cm⁻¹ and with a resolution of 4 cm⁻¹; 200 scans were collected for each spectrum. The ultimate analyses of elemental analysis were performed with an Elemental Analyzer (HEKAtech CHNS, Germany). The results were obtained as percentages of carbon, hydrogen, and nitrogen, and the oxygen content was determined indirectly by difference to 100%. Thermogravimetric-hyperdifferential scanning calorimetric (TG-HDSC) analyses were performed using a thermal analyzer (LINSEIS STA PT-1000, Germany) at a heat rate of 10°C·min⁻¹ starting from room temperature to a maximum temperature of 700°C under air atmosphere. X-ray diffraction analyses were carried out using a STOE Stadi-p X-ray powder diffractometer (STOE & Cie GmbH, Darmstadt, Germany) with CuKα radiation (40 kV, 30 mA and λ = 0.54056 Å). XRD patterns were recorded between 0° and 70° 2θ°, ranging in steps of 0.033° with a counting time per step of 200 s and with a scanning rate of 5° min⁻¹. SEM pictures were taken using a scanning electron microscope (Amray 1610 Turbo, USA).

2.2. Batch Adsorption and Desorption Studies. The stock solutions were prepared at a concentration of 1 × 10⁻³ mol·L⁻¹ by dissolving an accurately weighed amount of 0.2332 g of sodium salt of indigo carmine or of 0.1631 g of the hydrated sodium salt of 2,6-dichlorophenolindophenol in 500 mL of distilled water. The experimental solutions (1 × 10⁻⁵–1 × 10⁻⁴ mol·L⁻¹) were prepared by diluting the stock solutions with distilled water. The pH of each dye solutions was adjusted to the required value along the experiment by using small aliquots of HCl or NaOH solutions.

In this study, all adsorption studies were achieved in aqueous solution and at room temperature of 24.5°C. Batch

adsorption experiments were implemented in a set of well-adapted flasks in which various preweighted amounts (1–14 mg) of biosorbent were contacted with 30 mL of dye solutions of various initial concentrations (1×10^{-5} – 1×10^{-4} mol·L⁻¹). The mixture was stirred on a mechanical platform shaker at a constant agitation speed of 150 rpm for a variable specific period of contact time between 2 and 60 min. Afterwards, the supernatant solutions obtained by filtrating the suspensions using the Whatman filter paper were analyzed by measuring the absorbance using UV-Vis Spectrophotometer (JENWAY) at a λ_{\max} of 610 nm for IC [23] and 600 nm for 2,6-DCPIP [3, 5]. The monitoring absorbance was converted to the corresponding final concentration by using linear regression equations of calibration curve obtained from the linear plots of absorbance versus initial dye concentration of standard solutions. The dye uptake at equilibrium q_e (mol·g⁻¹) and at time q_t (mol·g⁻¹), and the dye removal percentage (%_{ads}) was estimated using the following equations [3, 16, 24, 25]:

$$\begin{aligned} q_e &= \frac{(C_i - C_e)V_s}{m}, \\ q_t &= \frac{(C_i - C_t)V_s}{m}, \\ \%_{\text{ads}} &= \frac{(C_i - C_e)}{C_i} \times 100, \end{aligned} \quad (1)$$

where C_i (mol·L⁻¹) is the initial dye concentration, C_e (mol·L⁻¹) is the equilibrium final dye concentration, C_t is the final dye concentration at time t , V_s (L) is the dye solution volume, and m (g) is the biosorbent weight.

For the desorption studies, 20 mg of CTAB-modified POF was combined in a flask with 100 mL of each dye solution at an initial concentration of 5×10^{-5} mol·L⁻¹. After stirring the mixtures at a constant agitation speed of 150 rpm for a period of 40 min for IC and 30 min for 2,6-DCPIP, the suspensions were filtered using the Whatman filter paper and the supernatant solutions obtained were analyzed by measuring the absorbance using UV-Vis Spectrophotometer. The dyes loaded with CTAB-modified POF, were collected after filtration, and were dried in an oven at 60°C, and 4 mg of each of these materials was contacted with 30 mL of desorption solutions of H₂O and 1×10^{-4} mol·L⁻¹ of NaOH or HNO₃. Afterwards, the mixtures were also stirred in the same condition as described earlier and the suspensions were again filtered. The supernatant solutions were also analyzed as described earlier in view to determine the desorbed dye concentration. The desorption percentages (%_{des}), translating the fraction of dyes released by the material, were determined as follows [3, 26]:

$$\%_{\text{des}} = \frac{C_f - C_r}{C_f} \times 100, \quad (2)$$

where C_f (mol·L⁻¹) is the initial concentration of dyes loaded with CTAB-modified POF and C_r (mol·L⁻¹) is the final concentration of dyes loaded with CTAB-modified POF.

2.3. Error Analysis. The nonlinear regression coefficient of determination (r^2) and chi-square test (χ^2) were used to evaluate the applicability of adsorption isotherm models. The expressions of the error functions are given as follows [27–30]:

$$\begin{aligned} \chi^2 &= \sum_1^N \frac{(q_{e,\text{exp}} - q_{e,\text{cal}})^2}{q_{e,\text{cal}}}, \\ r^2 &= \frac{\sum_1^N (q_{e,\text{cal}} - \overline{q_{e,\text{exp}}})^2}{\sum_1^N (q_{e,\text{cal}} - \overline{q_{e,\text{exp}}})^2 + \sum_1^N (q_{e,\text{cal}} - q_{e,\text{exp}})^2}, \end{aligned} \quad (3)$$

where $q_{e,\text{exp}}$ and $q_{e,\text{cal}}$ ($\mu\text{mol}\cdot\text{g}^{-1}$) are the equilibrium capacity of adsorption obtained from the experiment and by calculating from the model, respectively. N is the number of observations in the regression model (the number of data points).

3. Results and Discussion

3.1. Characterization of Biosorbent

3.1.1. Fourier-Transform Infrared (FT-IR) Spectroscopy. The FT-IR spectrum examination of raw POF was undertaken in order to locate the surface chemical functional groups, as shown in Figure 1(a). The spectrum exhibits the presence of a broad peak in the region 3400–3200 cm⁻¹, characteristics of the OH group, indicating the presence of alcohol, phenol, or carboxylic acids [3, 31, 32]. The band at 2890 cm⁻¹ was assigned to the presence of asymmetric and symmetric vibrations of CH₂. The carbonyl (C=O) of carboxylic acids and carboxylate groups occurred, respectively, at 1730 cm⁻¹ and 1613 cm⁻¹. Another absorption peak at 1238 cm⁻¹ could be attributed to C-O, C-H, or C-C stretching vibrations of carboxyl acid groups (-COOH). The maximum adsorption band localized around 1033 cm⁻¹ is probably due to C-O stretching vibrations of lignin [3, 31, 32].

The FT-IR spectrum of NaOH-treated POF (Figure 1(b)) reveals that the peaks at 1730 cm⁻¹ and 1238 cm⁻¹ located in raw POF disappeared after NaOH treatment. Moreover, the peak observed at 1613 cm⁻¹ changed from lower intensity peak in the IR spectrum of raw POF to higher intensity peak in the IR spectrum of NaOH-treated POF [32–34].

Compared to the FT-IR spectrum of NaOH-treated POF (Figure 1(b)), the FT-IR spectrum of CTAB-modified POF (Figure 1(c)) reveals the presence of new peaks at wavelength bands of 2921 cm⁻¹ and 2852 cm⁻¹. These bands are associated with the symmetric and asymmetric stretching vibrations of the methylene (CH₂) and methyl group (CH₃) of the aliphatic chain of the surfactant. Furthermore, another new peak of weak intensity appeared at 1462 cm⁻¹, which was attributed to methyl groups of the cationic substituent [7, 20, 21].

3.1.2. Thermogravimetric-Hyperdifferential Scanning Calorimetry (TG-HDSC). The thermal analyses of raw, NaOH-treated, and CTAB-modified POF were performed in terms

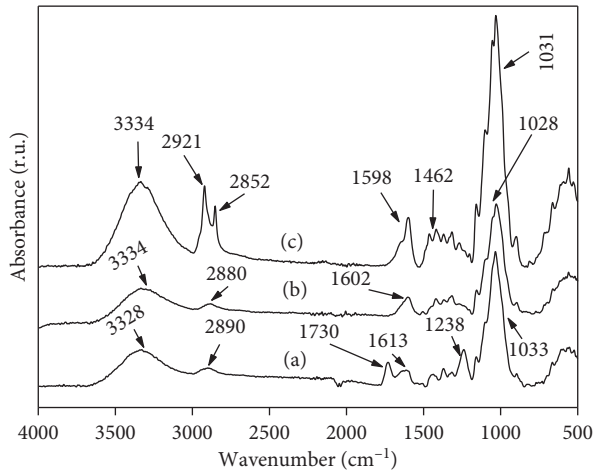


FIGURE 1: FT-IR spectra of (a) raw POF, (b) NaOH-treated POF, and (c) CTAB-modified POF.

of TG-HDSC curves. As shown in Figure 2(a), the TG-HDSC curves of raw POF suggest four typical distinct weight losses. The first weight loss of 8.92% located around 67°C over a temperature range of 26°C–200°C was attributed to the dehydration or loss of physically adsorbed water and water molecules. The second weight loss of 42.89% within the temperature range of 200°C–300°C may be due to the predominant decomposition of hemicelluloses, followed by a third high weight loss of 30.64% in the range of 300°C–350°C which was attributed to decomposition of cellulose. The last small weight loss of 2.52% above 350°C and located around 438°C was mostly due to decomposition of lignin [35–38].

The TG-HDSC curves of NaOH-treated POF (Figure 2(b)) also exhibited four typical distinct weight losses, which correspond to the thermal decomposition of the same elements in raw POF. The first weight loss of 10.89%, which occurred over a temperature interval of 26°C–200°C, was due to adsorbed water. The second weight loss of 69.51% over a temperature range of 200°C–310°C was due to the elimination of hemicellulose. The third weight loss of 12.49% within a temperature range of 310°C–420°C was due to the thermal alteration of cellulose. The last weight loss of 1.01% above 420°C was due to the thermal degradation of lignin.

In order to verify the effective modification of NaOH-treated POF by CTAB, the thermal analysis characterization of CTAB-modified POF was also performed and the results showed that the TG-HDSC curves of CTAB-modified POF (Figure 2(c)) exhibited five typical distinct weight losses. The first weight loss of 7.36%, which occurred over a temperature interval of 26°C–200°C was due to adsorbed water. The decrease in the first weight loss of CTAB-modified POF (7.36%) compared to NaOH-treated POF (10.89%) is due to the hydrophobic nature of POF after insertion of the CTAB in the interlayer of this biosorbent. The second weight loss of 20.41% over a temperature range of 200°C–250°C was due to the elimination of hemicellulose. The third weight loss of 27.10% over a temperature interval of 250°C–330°C which

was absent on the curves of NaOH-treated POF was related to the evaporation/decomposition of the loaded surfactants (CTAB; whose melting point is between 248°C and 251°C) in the interlayer of biosorbent [19, 22]. The fourth weight loss of 13.39% within a temperature range of 250°C–300°C was due to the thermal alteration of cellulose. The last weight loss above 480°C that is nonsignificant was due to the thermal degradation of lignin.

3.1.3. Scanning Electron Microscopy (SEM). Scanning electron microscopy of raw, NaOH-treated, and CTAB-modified POF was carried out in view to assess the effect of NaOH treatment and CTAB modification on the surface morphology of POF. As shown in Figures 3(a) and 3(b), the surface morphology of raw POF presents an irregular shape and a porous surface. After NaOH treatment (Figures 3(c) and 3(d)), the biosorbent (NaOH-treated POF) has a spongy morphology with a porosity more developed due to the action of NaOH on POF that promotes highest weight losses of biosorbent which leads to an increase in internal surface area and also favors the development of pores [39, 40]. The SEM image of CTAB-modified POF (Figures 3(e) and 3(f)) exhibited a surface almost smooth, more compact, or again that contains very few pores due to the fact that the external surface of CTAB-modified POF was covered by a CTAB thin film [7].

3.1.4. X-Ray Diffraction Analysis (XRD). X-ray diffraction technique is a powerful tool used to investigate the crystalline nature of materials. As shown in Figure 4(a), in the X-ray diffraction pattern of raw POF, the peaks are observed at the 16°, 22.5°, and 34.5° 2θ angles, corresponding to the cellulose I structure. These peaks are indicative of highly organized crystalline cellulose [41, 42]. The last-mentioned peaks are also observed in the XRD pattern of NaOH-treated (Figure 4(b)) and CTAB-modified POF (Figure 4(c)), indicating that the crystal structure remains stable after NaOH treatment and CTAB modification processes.

3.1.5. Elemental Analysis. The elemental analyses of raw, NaOH-treated, and CTAB-modified POF are illustrated in Table 1. As shown in Table 1, the raw POF is composed of 42.282% carbon, 6.276% hydrogen, 0.788% nitrogen, and 50.654% oxygen. After the NaOH treatment, the biosorbent is composed of the same chemical elements: 40.532% carbon, 6.161% hydrogen, 0.263% nitrogen, and 53.044% oxygen. It can be observed that the percentages of carbon, hydrogen, and nitrogen of NaOH-treated POF are lower than those of raw POF, while the oxygen percentage of NaOH-treated POF is higher than that of raw POF. A similar trend was also obtained for the NaOH treatment of olive tree pruning by Calero et al. [39] and Ronda et al. [43]. Likewise, after the CTAB modification, the biosorbent is also composed of the same chemical elements: 49.236% carbon, 8.006% hydrogen, 1.229% nitrogen, and 41.529% oxygen. It can also be observed that the percentages of carbon, hydrogen, and nitrogen for CTAB-modified POF are higher

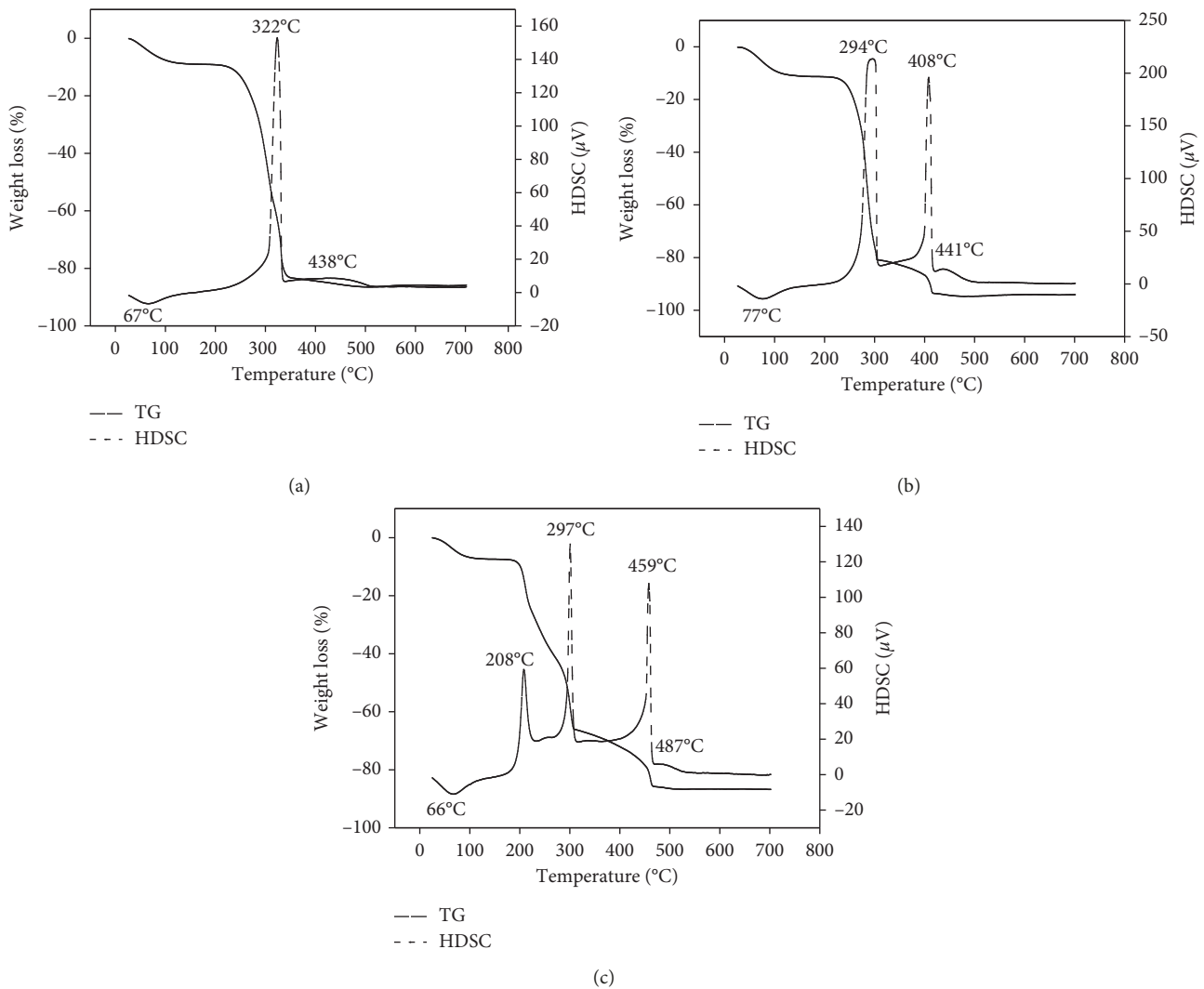


FIGURE 2: TG-HDSC curves of (a) raw POF, (b) NaOH-treated POF, and (c) CTAB-modified POF.

than those of NaOH-treated POF, while the oxygen percentage of CTAB-modified POF is lower than that of NaOH-treated POF. This increase in carbon, hydrogen, and nitrogen percentages is expected due to the loading of CTAB in the NaOH-treated POF interlayer [44].

3.2. Effect of Modification of Biosorbent. The biosorbent was first of all treated with NaOH to be modified by CTAB. Figure 5 shows the effect of chemical modification on the adsorption of IC and 2,6-DCPIP. The amount of dyes adsorbed at equilibrium is higher with CTAB-modified POF (219.07 and 109.686 $\mu\text{mol}\cdot\text{g}^{-1}$ for IC and 2,6-DCPIP, respectively) than that obtained with raw POF (1.898 and 1.450 $\mu\text{mol}\cdot\text{g}^{-1}$ for IC and 2,6-DCPIP, respectively). This result can be explained by the fact that the NaOH treatment promotes high weight losses and hydrolysis reactions that cause high dissolution of organic substances from the biomass. These hydrolysis reactions lead to the formation of more carboxylate ($-\text{COO}^-$) groups in the NaOH-treated biomass [32, 33, 39], which enhance the cationic surfactant

fixation by electrostatic attraction. In addition, NaOH treatment of raw POF causes the swelling of material which leads to an increase in the internal surface area and also favors the cationic surfactant fixation [12]. The increase in cationic surfactant fixation after NaOH treatment of raw POF could also be due to the destruction of autolytic enzymes causing putrefaction of biomass and the removal of lipids and proteins as well as polysaccharides that mask binding sites [32, 45]. The results of the adsorption of IC and 2,6-DCPIP onto CTAB-modified NaOH-treated POF and CTAB-modified raw POF (figure not shown here) were 219.070 and 140.098 $\mu\text{mol}\cdot\text{g}^{-1}$ for IC and 109.686 and 58.028 $\mu\text{mol}\cdot\text{g}^{-1}$ for 2,6-DCPIP, respectively. This indicates that CTAB-modified NaOH-treated POF has higher adsorption capacities than CTAB-modified raw POF due to the NaOH treatment.

Secondly, the modification of POF by CTAB covered the surface of cell walls by cationic surfactant which increased new functional groups on the POF surfaces and facilitated the formation of hydrogen bonding and electrostatic interaction between the positively charged surface of the

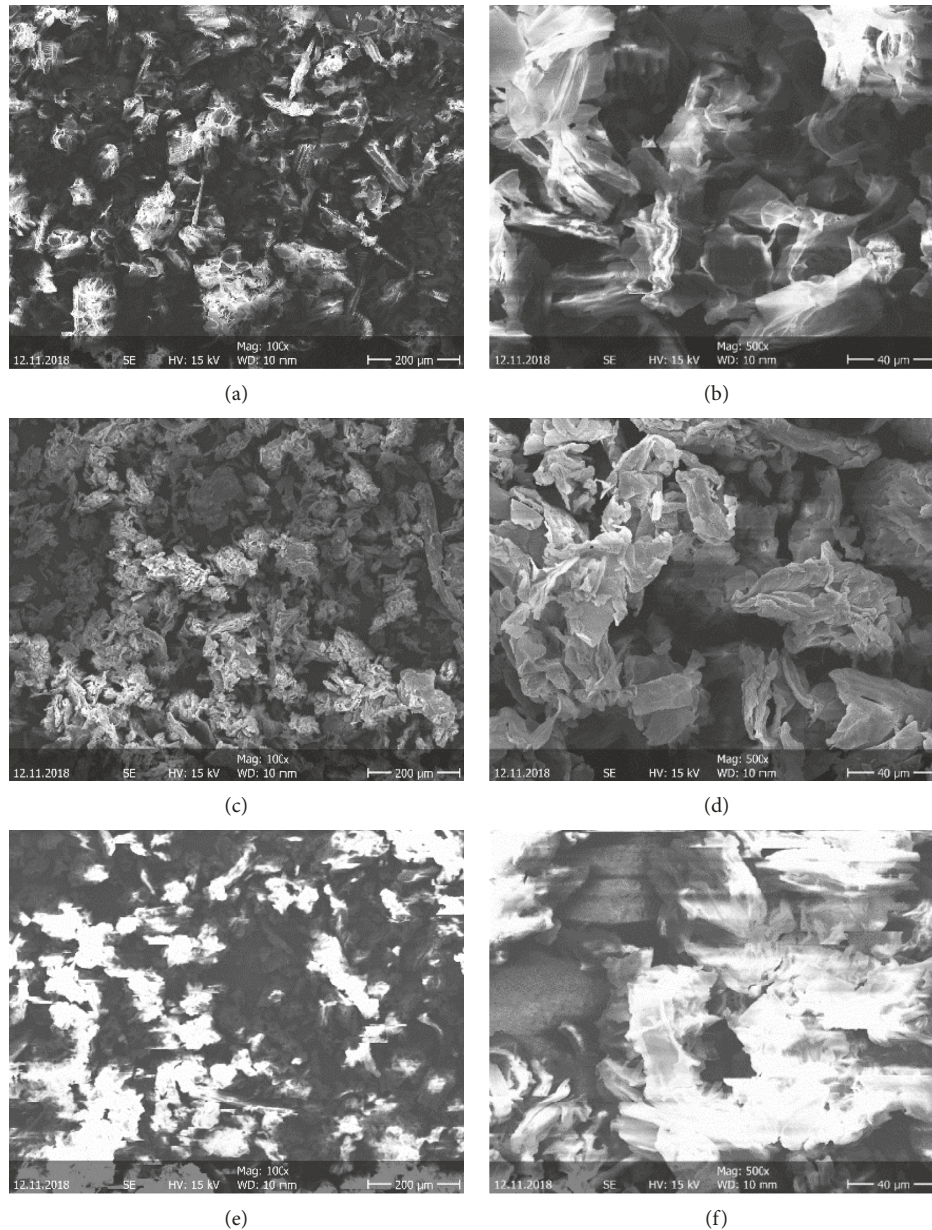


FIGURE 3: SEM images of (a, b) raw POF, (c, d) NaOH-treated POF, and (e, f) CTAB-modified POF.

material and the negatively charged molecules of anionic dyes (Figure 6) [7]. In addition, when the CTAB is inserted into the POF interlayer, the POF became hydrophobic, improving its adsorption capacity [19, 21].

3.3. Effect of Biosorbent Dosage. The effect of biosorbent dosage on the removal of IC and 2,6-DCPIP at an initial dye concentration was studied, and the results are shown in Figure 7. The removal percentage of IC and 2,6-DCPIP increased up to 99.696% and 76.589%, respectively. As can be seen, the percentage of adsorption increased with increasing adsorbent dosage. This can be explained by the fact that the increase in adsorbent dosage involves a greater surface area and more availability of free adsorption

sites for dye adsorption during the adsorption reaction [25, 46, 47].

3.4. Effect of Contact Time. The effect of contact time (2–60 min) on adsorption of IC and 2,6-DCPIP is presented in Figure 8. Rapid adsorption of IC and 2,6-DCPIP takes place in the first 2 minutes for the two dyes; thereafter, the adsorption rate gradually reduces with the increasing adsorption time until reaching equilibrium in about 30 minutes for IC ($222.107 \mu\text{mol}\cdot\text{g}^{-1}$) and 20 minutes for 2,6-DCPIP ($102.306 \mu\text{mol}\cdot\text{g}^{-1}$). Beyond the equilibrium time, we observed no significant change in dye removal. The initial rapid phase may be attributed to rapid dye attachment on the CTAB-modified POF surface due to either the

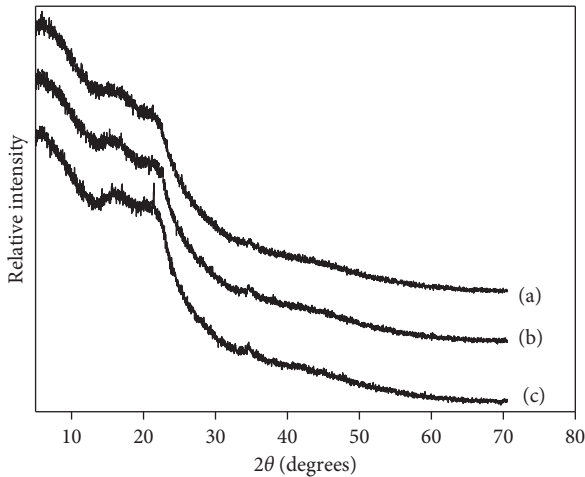


FIGURE 4: XRD curves of (a) raw POF, (b) NaOH-treated POF, and (c) CTAB-modified POF.

TABLE 1: Elemental analysis of raw, NaOH-treated, and CTAB-modified POF.

Biosorbents	Elemental composition (%)			
	C	H	N	O
Raw POF	42.282	6.276	0.788	50.654
NaOH-treated POF	40.532	6.161	0.263	53.044
CTAB-modified POF	49.236	8.006	1.229	41.529

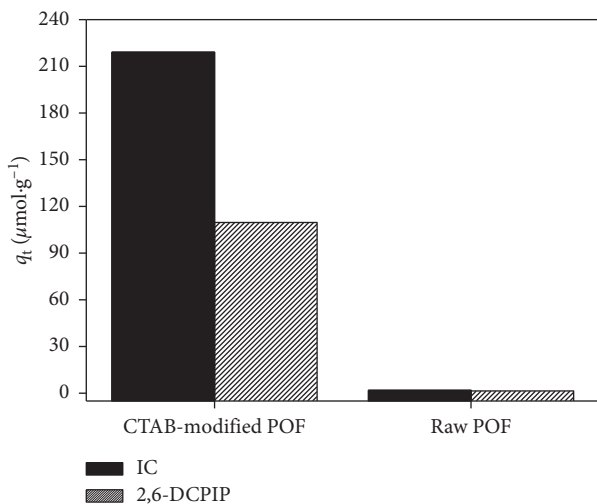


FIGURE 5: Effect of CTAB-modified POF on the IC and 2,6-DCPIP adsorption. Experimental conditions: $[IC] = [2,6\text{-DCPIP}] = 5 \times 10^{-5} \text{ mol}\cdot\text{L}^{-1}$; $m = 0.133 \text{ g}\cdot\text{L}^{-1}$; $G = 0\text{--}100 \mu\text{m}$; $t = 60 \text{ min}$; $\nu = 150 \text{ rpm}$; $V = 30 \text{ mL}$; $\text{pH} = 6.2$ for IC and $\text{pH} = 6.7$ for 2,6-DCPIP; at room temperature.

large amount of surface area available or to the availability of more adsorption vacant sites at the initial stage. Subsequently, the lowering of the rate of the adsorption is due to the decrease in the total adsorbent surface area and less available binding sites [1, 17]. No change in the amount of dye adsorbed after the equilibrium period is due to the

saturation of the adsorption active sites by the dye molecules [1, 25, 48].

3.5. Effect of Initial Dye Concentration. The effect of initial concentration on the adsorption of IC and 2,6-DCPIP was investigated in the range of $10\text{--}100 \mu\text{mol}\cdot\text{L}^{-1}$. As shown in Figure 9, the amount of IC and 2,6-DCPIP adsorbed at equilibrium increases from 79.176 to $298.191 \mu\text{mol}\cdot\text{g}^{-1}$ and from 5.249 to $120.209 \mu\text{mol}\cdot\text{g}^{-1}$, respectively. The amount adsorbed at equilibrium increases with the concentration of both dyes. This result can be explained by the fact that increasing the initial dye concentration would increase the mass transfer driving force, i.e., concentration gradient, and also favor the rate at which dye molecules pass from solution to the particle surface [4, 9, 25]. This behaviour suggests that available sites on the biosorbent surface are the limiting factor for the IC and 2,6-DCPIP removal [3, 17].

3.6. Effect of Solution pH. The effect of initial solution pH on adsorption of IC and 2,6-DCPIP onto CTAB-modified POF is shown in Figure 10, and the results indicate that when the pH increases, the capacity of adsorption decreases from 410.804 to $206.426 \mu\text{mol}\cdot\text{g}^{-1}$ and from 338.458 to $49.418 \mu\text{mol}\cdot\text{g}^{-1}$ for IC and 2,6-DCPIP dyes, respectively. This can be explained by the fact that the point of zero charge (PZC, determined by the method described in our previous work by Ngaha et al. [3]) of CTAB-modified POF is 6.6; thus, at low pH ($\text{pH} < \text{PZC}$), more protons will be available for the biosorbent surface protonation, which increases the electrostatic attraction between the positively charged biosorbent sites and the negatively charged dyes. At lower pH ($\text{pH} = 2$), there is nearly no electrostatic repulsion between the biosorbent and the dyes; hence, the amount adsorbed is at its maximum. Increasing the pH ($\text{pH} > \text{PZC}$) favors the raise in hydroxyl ions, which lead to an increase in dye anions in the solution as well as the number of negatively charged sites on the adsorbent surface. This results in electrostatic repulsion between the dyes and CTAB-modified POF, which is the reason for the decrease in the adsorption capacity [3, 49, 50].

3.7. Effect of Ionic Strength. The effect of ionic strength on adsorption of IC and 2,6-DCPIP onto CTAB-modified POF was analyzed in the NaCl solutions with concentrations ranging from 0.000 to $0.060 \text{ mol}\cdot\text{L}^{-1}$, and the results are illustrated in Figure 11. When the ionic strength increased, the adsorption capacity of IC increased (from 221.348 to $385.366 \mu\text{mol}\cdot\text{g}^{-1}$) and the adsorption capacity of 2,6-DCPIP is not affected ($\approx 97.784 \mu\text{mol}\cdot\text{g}^{-1}$). The increase in IC adsorption capacity can be attributed to the fact that the addition of salt (NaCl) favors the aggregation of IC molecules and decreases its solubility [3, 51, 52]. Another explanation is that the positive charge surface of biosorbent increases with increasing ionic strength, which leads to an increase in electrostatic attraction between IC ions and CTAB-modified

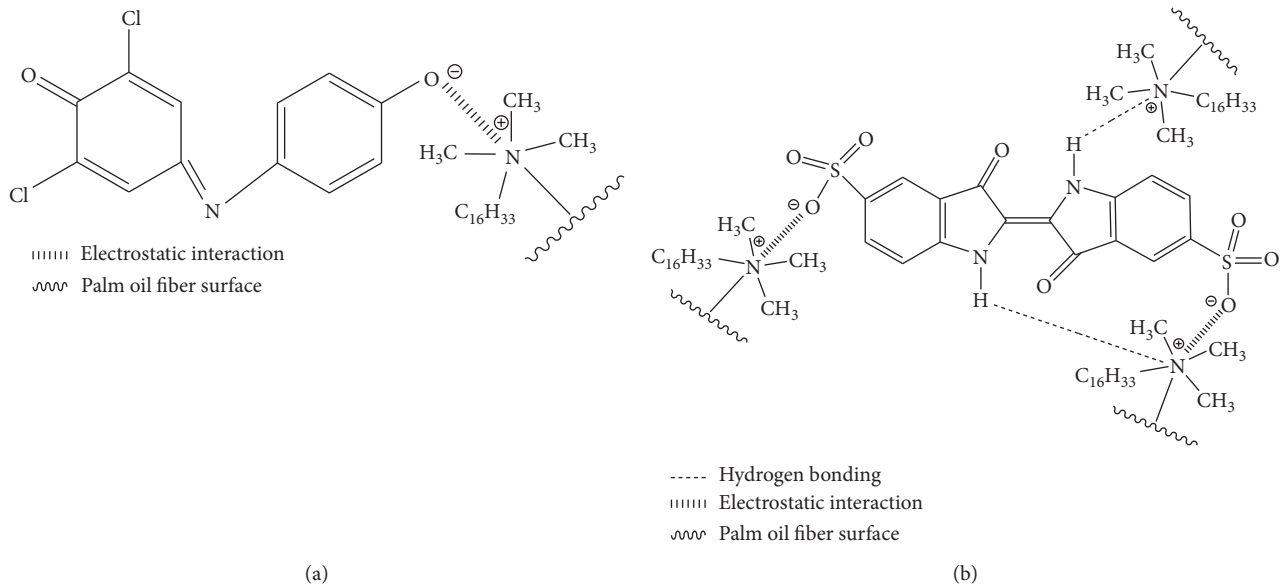


FIGURE 6: Schematic representation of adsorption mechanisms of (a) 2,6-DCPIP and (b) IC onto CTAB-modified POF.

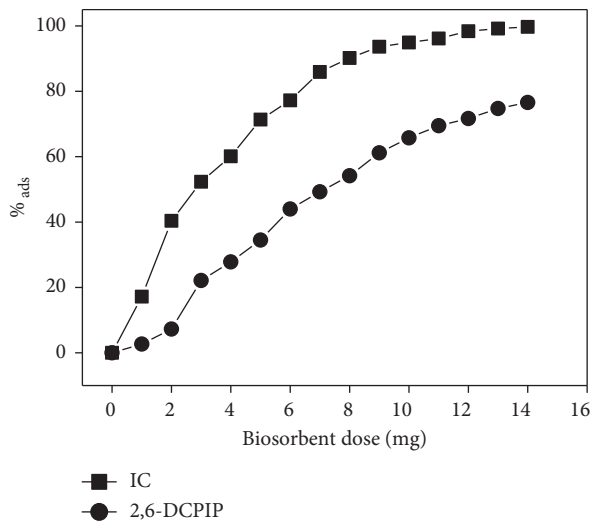


FIGURE 7: Effect of biosorbents dose on the IC and 2,6-DCPIP adsorption. Experimental conditions: $[IC] = [2,6-DCPIP] = 5 \times 10^{-5} \text{ mol}\cdot\text{L}^{-1}$; $G = 0-100 \mu\text{m}$; $t = 40 \text{ min}$ and $\text{pH} = 6.2$ for IC; $t = 30 \text{ min}$ and $\text{pH} = 6.7$ for 2,6-DCPIP; $v = 150 \text{ rpm}$; $V = 30 \text{ mL}$; at room temperature.

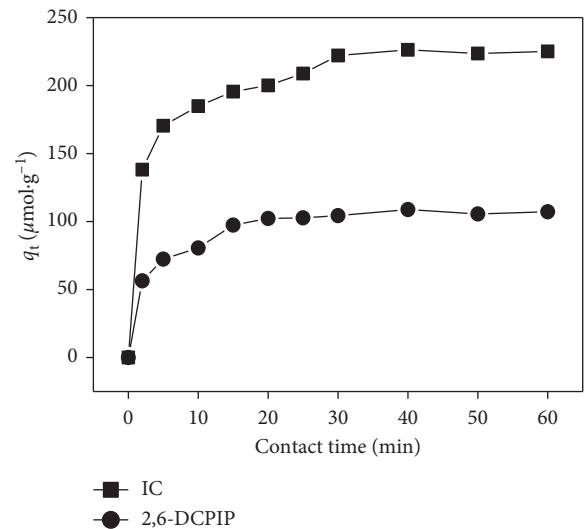


FIGURE 8: Effect of contact time on the IC and 2,6-DCPIP adsorption. Experimental conditions: $[IC] = [2,6-DCPIP] = 5 \times 10^{-5} \text{ mol}\cdot\text{L}^{-1}$; $m = 0.133 \text{ g}\cdot\text{L}^{-1}$; $G = 0-100 \mu\text{m}$; $v = 150 \text{ rpm}$; $V = 30 \text{ mL}$; $\text{pH} = 6.2$ for IC and $\text{pH} = 6.7$ for 2,6-DCPIP; at room temperature.

POF [3, 53]. Secondly, the insignificant change in 2,6-DCPIP adsorption capacity may be due to the fact that chlorine and sodium ions have no effect on adsorption of 2,6-DCPIP onto CTAB-modified POF [54].

3.8. Adsorption Isotherm Models

3.8.1. Langmuir Isotherm. The general formulas of nonlinear (equation (4)) and linear (equation (5)) expressions of the Langmuir isotherm are, respectively, illustrated as follows [14, 55]:

$$q_e = \frac{K_L q_{\max} C_e}{1 + K_L C_e}, \quad (4)$$

$$\frac{C_e}{q_e} = \frac{1}{K_L \cdot q_{\max}} + \frac{C_e}{q_{\max}}, \quad (5)$$

where q_{\max} ($\mu\text{mol}\cdot\text{g}^{-1}$) is the maximum adsorption capacity of CTAB-modified POF, q_e ($\mu\text{mol}\cdot\text{g}^{-1}$) is the equilibrium adsorption capacity of CTAB-modified POF, C_e ($\mu\text{mol}\cdot\text{L}^{-1}$) is the concentration of dye solutions at equilibrium, and K_L ($\text{L}\cdot\mu\text{mol}^{-1}$) is the Langmuir adsorption

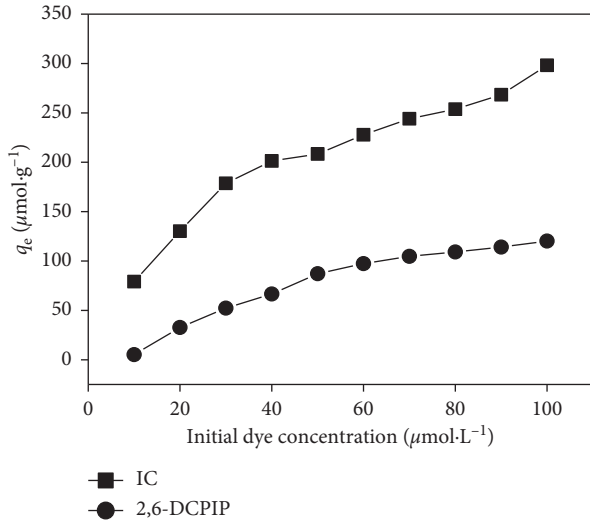


FIGURE 9: Effect of initial concentration on the IC and 2,6-DCPIP adsorption. Experimental conditions: $m = 0.133 \text{ g}\cdot\text{L}^{-1}$; $G = 0\text{--}100 \mu\text{m}$; $t = 40 \text{ min}$ and $\text{pH} = 6.2$ for IC; $t = 30 \text{ min}$ and $\text{pH} = 6.7$ for 2,6-DCPIP; $\nu = 150 \text{ rpm}$; $V = 30 \text{ mL}$; at room temperature.

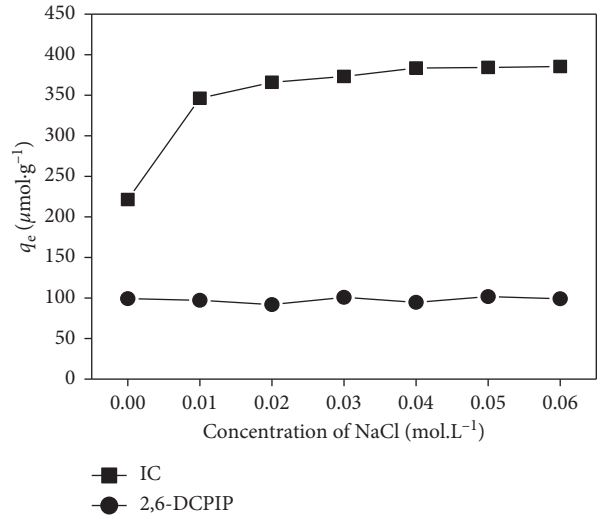


FIGURE 11: Effect of ionic strength on the IC and 2,6-DCPIP adsorption. Experimental conditions: $[\text{IC}] = [\text{2,6-DCPIP}] = 5 \times 10^{-5} \text{ mol}\cdot\text{L}^{-1}$; $m = 0.133 \text{ g}\cdot\text{L}^{-1}$; $G = 0\text{--}100 \mu\text{m}$; $t = 40 \text{ min}$ and $\text{pH} = 6.2$ for IC; $t = 30 \text{ min}$ and $\text{pH} = 6.7$ for 2,6-DCPIP; $\nu = 150 \text{ rpm}$; $V = 30 \text{ mL}$; at room temperature.

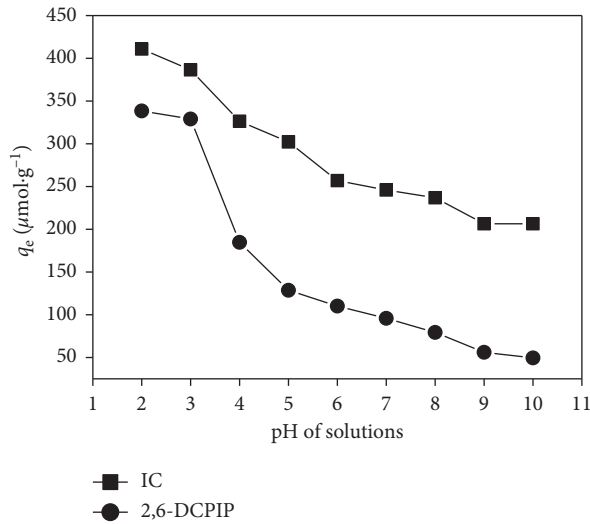


FIGURE 10: Effect of solution pH on the IC and 2,6-DCPIP adsorption. Experimental conditions: $[\text{IC}] = [\text{2,6-DCPIP}] = 5 \times 10^{-5} \text{ mol}\cdot\text{L}^{-1}$; $m = 0.133 \text{ g}\cdot\text{L}^{-1}$; $G = 0\text{--}100 \mu\text{m}$; $t = 40 \text{ min}$ for IC; $t = 30 \text{ min}$ for 2,6-DCPIP; $\nu = 150 \text{ rpm}$; $V = 30 \text{ mL}$; at room temperature.

equilibrium constant. The linear plots of C_e/q_e versus C_e allowed to determine q_{max} and K_L constant values from their slopes and intercepts, respectively. The separation factor (R_L) is defined using the following equation [3, 56]:

$$R_L = \frac{1}{1 + K_L C_i} \quad (6)$$

The R_L value indicates whether the shape of the adsorption isotherm will be either favorable ($0 < R_L < 1$), unfavorable ($R_L > 1$), linear ($R_L = 1$), or irreversible ($R_L = 0$).

3.8.2. *Freundlich Isotherm.* The general formulas of non-linear (equation (7)) and linear (equation (8)) expressions of the Freundlich isotherm are, respectively, described as follows [14, 55]:

$$q_e = K_f C_e^{1/n}, \quad (7)$$

$$\text{Log } q_e = \text{log } K_f + \frac{1}{n} \text{log } C_e, \quad (8)$$

where $K_f (\text{L}\cdot\text{g}^{-1})$ is the Freundlich constant taken as an indicator of adsorption capacity and $1/n$ is a measure related to the adsorption intensity of the CTAB-modified POF. The linear plots of $\text{log } q_e$ versus $\text{log } C_e$ allowed to determine the $1/n$ and K_f constant values from their slopes and intercepts, respectively.

3.8.3. *Dubinin–Radushkevich Isotherm.* The general formulas of nonlinear (equation (9)) and linear (equation (10)) equations of the Dubinin–Radushkevich isotherm are, respectively, illustrated by the following expressions [16, 57]:

$$q_e = q_{\text{max}} e^{-\beta \epsilon^2}, \quad (9)$$

$$\ln q_e = \ln q_{\text{max}} - \beta \epsilon^2, \quad (10)$$

where $\beta (\text{mol}^2\cdot\text{kJ}^{-2})$ is the activity coefficient related to the mean free energy ($E (\text{kJ}\cdot\text{mol}^{-1})$) and ϵ is Polanyi potential calculated from the following equation:

$$\epsilon = RT \ln \left(1 + \frac{1}{C_e} \right), \quad (11)$$

$$E = \frac{1}{\sqrt{-2\beta}}$$

where R ($8.314 \times 10^{-3} \text{ kJ}\cdot\text{mol}^{-1}\cdot\text{K}^{-1}$) and T (298 K) are the universal gas constant and the absolute temperature, respectively. The constant values of β and q_{\max} were evaluated, respectively, from the slopes and intercepts of straight lines obtained by plotting $\ln q_e$ versus ϵ^2 .

3.8.4. Temkin Isotherm. The general formulas of nonlinear (equation (12)) and linear (equation (13)) equations of the Temkin isotherm are, respectively, given by the following expressions [28, 55, 57, 58]:

$$q_e = q_{\max} \frac{RT}{\Delta Q} \ln K_T C_e, \quad (12)$$

$$q_e = q_{\max} \frac{RT}{\Delta Q} \ln K_T + q_{\max} \frac{RT}{\Delta Q} \ln C_e, \quad (13)$$

where ΔQ ($\text{kJ}\cdot\text{mol}^{-1}$) and K_T ($\text{L}\cdot\mu\text{mol}^{-1}$) are the adsorption heat and the Temkin isotherm constant, respectively. The constant values of ΔQ and K_T were determined from the slopes and the intercepts of straight lines obtained by plotting q_e versus $\ln C_e$, respectively.

The nonlinear regression and separation factor graphs of adsorption isotherms obtained for IC and 2,6-DCPIP adsorption onto CTAB-modified POF are shown in Figure 12. The corresponding constants obtained from the nonlinear regressions are recapped in Table 2.

The data of Table 2 indicate that the values of coefficient of determination of the Freundlich isotherm ($r^2 = 0.953$) for IC and Temkin isotherm ($r^2 = 0.986$) for 2,6-DCPIP are closest to unity, implying that Freundlich and Temkin isotherms are most appropriate to describe the adsorption of IC and 2,6-DCPIP on CTAB-modified POF, respectively. This is also confirmed by the low values of chi-square test error obtained with the Freundlich isotherm ($\chi^2 = 4.398$) for IC and Temkin isotherm ($\chi^2 = 1.196$) for 2,6-DCPIP. The good fit of IC experimental equilibrium data to the Freundlich isotherm indicates the multilayer coverage with heterogeneous sorption sites and different fixing energies of IC onto CTAB-modified POF [16, 58].

It is difficult to compare the maximum adsorption capacity values determined by the Langmuir model of different types of adsorbents because the experimental conditions used are not identical. Table 3 summarizes the comparison of the maximum IC and 2,6-DCPIP adsorption capacities of various adsorbents including CTAB-modified POF. The comparison shows that CTAB-modified POF has higher adsorption capacity of IC ($128.444 \text{ mg}\cdot\text{g}^{-1}$) and 2,6-DCPIP ($75.143 \text{ mg}\cdot\text{g}^{-1}$) than many of the other reported adsorbents, reflecting a promising future for CTAB-modified POF utilization in IC and 2,6-DCPIP removal from aqueous solutions.

The values of $1/n$ evaluated from the Freundlich model (0.231 for IC and 0.629 for 2,6-DCPIP) are less than unity, meaning that adsorption is favorable for both dyes [3, 14, 55]. The adsorption energy obtained from the Dubinin–Radushkevich isotherm ($9.880 \text{ kJ}\cdot\text{mol}^{-1}$) lies in the range of 8 to $16 \text{ kJ}\cdot\text{mol}^{-1}$ for 2,6-DCPIP, implying that

anionic exchange is the mechanism that controls the adsorption process of 2,6-DCPIP [3, 57]. However, for IC ($17.165 \text{ kJ}\cdot\text{mol}^{-1}$), this value is higher than the range. The positive values of adsorption heat evaluated from the Temkin model (Table 2) indicate the exothermic character of the adsorption process [3, 53]. Moreover, the adsorption heat of IC ($14.935 \text{ kJ}\cdot\text{mol}^{-1}$) is greater than the adsorption heat of 2,6-DCPIP ($10.712 \text{ kJ}\cdot\text{mol}^{-1}$). This may reflect the fact that interactions between IC ions and CTAB-modified POF are more energetic than interactions between 2,6-DCPIP ions and CTAB-modified POF [3, 58].

The separation factor values evaluated from the Langmuir model (Figure 12(c)) lie in the range 0–1 (0.036–0.270 for IC and 0.419–0.878 for 2,6-DCPIP), implying that adsorption is favorable for both dyes. This result corroborates with what was already observed with the Freundlich model. At higher initial dye concentrations, the R_L values are lower, showing that adsorption is more favorable at these concentrations for both dyes [3, 65]. The R_L values of IC are lower than those of 2,6-DCPIP, implying that the adsorption onto CTAB-modified POF is more favorable with IC rather than 2,6-DCPIP [56]. The R_L values also show that at high initial IC concentrations (0.036), the adsorption is nearly irreversible and at lower initial 2,6-DCPIP concentrations (0.878), the adsorption is nearly linear [66].

3.9. Adsorption Kinetic Models

3.9.1. Pseudo-First-Order Model. The linear form of the pseudo-first-order model of Lagergren is expressed using the following equation [3, 16, 67, 68]:

$$\log(q_e - q_t) = \log q_e - \frac{K_{1\text{ads}}}{2.303} t, \quad (14)$$

where q_e and q_t ($\mu\text{mol}\cdot\text{g}^{-1}$) are the amounts of dyes adsorbed on CTAB-modified POF at equilibrium and at contact time t , respectively. $K_{1\text{ads}}$ (min^{-1}) is the rate constant of pseudo-first-order model. The slopes and intercepts of the linear plots of $\log(q_e - q_t)$ versus t were used to estimate the constant values of $K_{1\text{ads}}$ and q_e , respectively.

3.9.2. Pseudo-Second-Order Model. The linear expression of pseudo-second-order model is presented in the following equation [3, 16, 67, 68]:

$$\frac{t}{q_t} = \frac{1}{K_{2\text{ads}} \cdot q_e^2} + \frac{1}{q_e} t, \quad (15)$$

where $K_{2\text{ads}}$ ($\text{g}\cdot\mu\text{mol}^{-1}\cdot\text{min}^{-1}$) is the rate constant of the pseudo-second-order model. The slopes and intercepts of the linear plots of t/q_t versus t were used to calculate the constant values of q_e and $K_{2\text{ads}}$, respectively. From this model, the initial rate of reaction h ($\mu\text{mol}\cdot\text{g}^{-1}\cdot\text{min}^{-1}$) (equation (16)) and the half time of the reaction $t_{1/2}$ (min) (equation (17)) were evaluated:

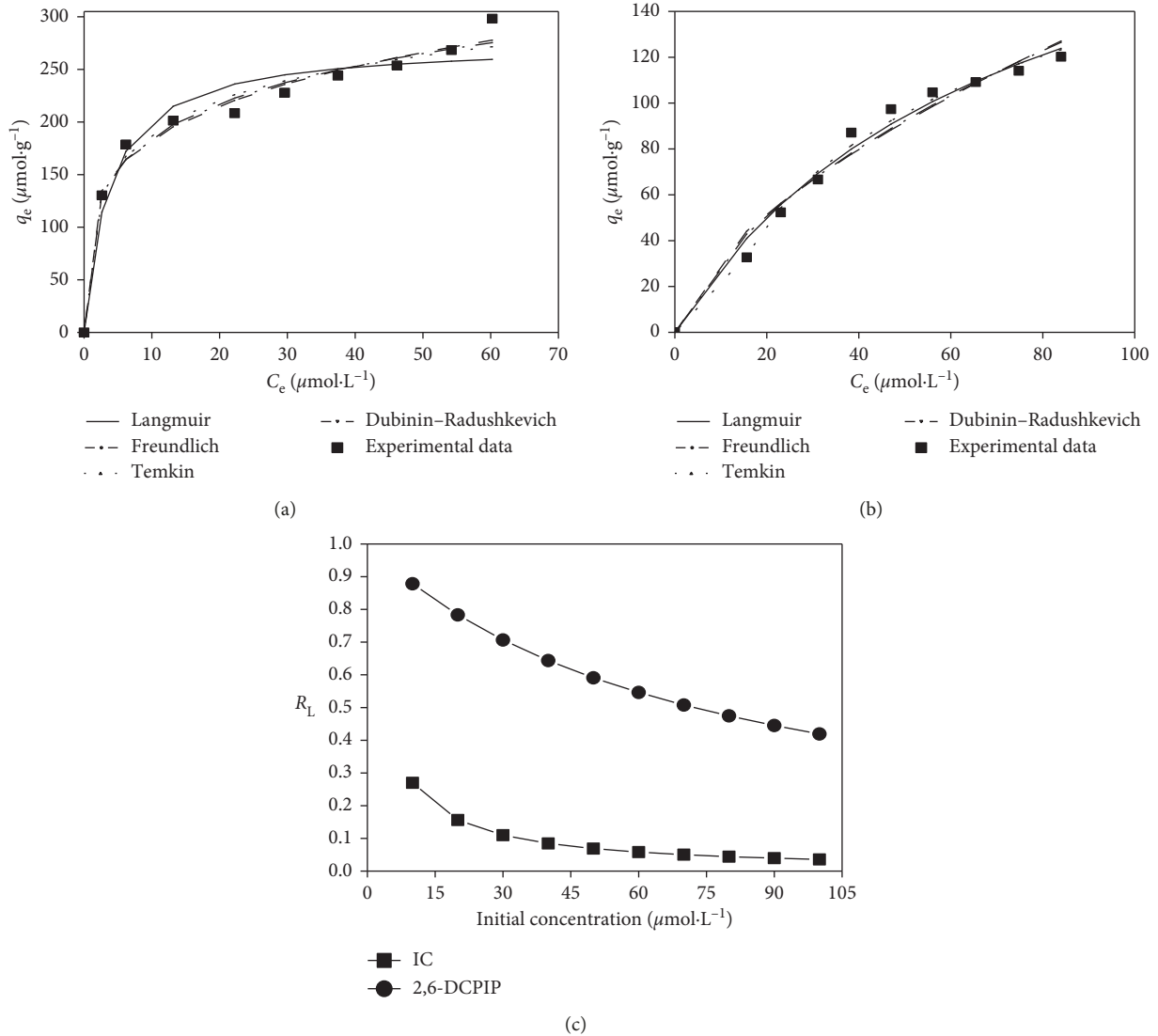


FIGURE 12: Variation in the adsorbed amount of (a) IC and (b) 2,6-DCPIP at equilibrium on CTAB-modified POF and (c) evolution of R_L values against the initial dye concentration.

$$h = K_{2_{\text{ads}}} \cdot q_e^2, \quad (16)$$

$$t_{1/2} = \frac{1}{q_e \cdot K_{2_{\text{ads}}}}. \quad (17)$$

3.9.3. *Elovich Model.* The linear expression of the Elovich model is represented by the following equation [3, 67, 69]:

$$q_t = \frac{1}{\beta} \ln(\alpha\beta) + \frac{1}{\beta} \ln t, \quad (18)$$

where α ($\mu\text{mol}\cdot\text{g}^{-1}\cdot\text{min}^{-1}$) is the initial adsorption rate and β ($\text{g}\cdot\mu\text{mol}^{-1}$) is related to the extent of surface coverage and activation energy for chemisorption. The slopes and intercepts of the linear plots of q_t versus $\ln t$ were used to determine the constant values of β and α , respectively.

3.9.4. *Intraparticle Diffusion Model.* The intraparticle diffusion model based on the theory proposed by Weber and Morris is usually expressed in terms of square root of time, as shown in the following equation [3, 14, 25, 67]:

$$q_t = K_{\text{ip}} t^{1/2} + C, \quad (19)$$

where K_{ip} ($\mu\text{mol}\cdot\text{g}^{-1}\cdot\text{min}^{-1/2}$) and C ($\mu\text{mol}\cdot\text{g}^{-1}$) are, respectively, the intraparticle diffusion rate constant and the thickness of the boundary layer. From the slopes and intercepts of straight lines obtained by plotting q_t versus $t^{1/2}$, the constant values of K_{ip} and C were estimated, respectively.

3.9.5. *External Mass Transfer Resistance Model.* This model is used to calculate the initial rate of solute sorption using the classical mass transfer equation [3, 14, 70]:

TABLE 2: Langmuir, Freundlich, Dubinin-Radushkevich, and Temkin parameters for IC and 2,6-DCPIP adsorption onto CTAB-modified POF.

Dyes	Langmuir			Freundlich			Dubinin-Radushkevich			Temkin					
	K_L ($L \cdot \mu\text{mol}^{-1}$)	q_{max} ($\mu\text{mol} \cdot \text{g}^{-1}$)	χ^2	K_f ($L \cdot \text{g}^{-1}$)	$1/n$	χ^2	E ($\text{kJ} \cdot \text{mol}^{-1}$)	q_{max} ($\mu\text{mol} \cdot \text{g}^{-1}$)	χ^2	Δq ($\text{kJ} \cdot \text{mol}^{-1}$)	KT ($L \cdot \mu\text{mol}^{-1}$)	χ^2	r^2		
IC	0.270	275.426	14.105	0.003	0.231	4.398	0.953	17.165	736.670	4.812	0.946	14.935	6.329	5.563	0.934
2,6-DCPIP	0.014	230.423	3.462	0.046	0.629	6.291	0.938	9.880	2018.255	5.306	0.948	10.712	0.120	1.196	0.986

TABLE 3: Comparison of maximum adsorption capacities of some adsorbent materials for IC and 2,6-DCPIP, from the literature.

Adsorbent materials	Adsorbate	q_{\max} (mg·g ⁻¹)	References
Palm oil fiber	IC	128.444	Present work
Pecan nut shells	IC	13.408	[59]
Calcium hydroxide	IC	0.950	[47]
Montmorillonite	IC	40.000	[60]
Fe-zeolitic tuff	IC	32.830	[61]
Carbonaceous material	IC	92.830	[61]
Chitin	IC	5.783	[62]
Chitosan	IC	71.818	[62]
Rice husk ash	IC	65.908	[46]
Layered double hydroxide	IC	55.500	[63]
Brazil nut shells	IC	1.090	[64]
Palm oil fiber	2,6-DCPIP	75.143	Present work
Palm tree trunk	2,6-DCPIP	51.299	[3]

$$\frac{dC_t}{dt} = -\beta_L S(C_t - C_s), \quad (20)$$

where β_L , C_t , C_s , and S are, respectively, the external mass transfer coefficient, the liquid-phase solute concentration at time t , the liquid-phase solute concentration at the particle surface and the specific surface area for mass transfer. The following equation is obtained by simplifying this equation [3, 14, 70]:

$$\frac{d(C_t/C_0)}{dt} = -\beta_L S. \quad (21)$$

The initial slope of the C_t/C_0 versus time graph was used to approximate the external mass transfer rate $\beta_L S$.

3.9.6. Boyd Model. The Boyd model is used to evaluate the rate-controlling step involved in the dye adsorption process [3, 14, 41, 55, 70]:

$$F = 1 - \frac{6}{\pi^2} \exp(-Bt). \quad (22)$$

Since $F = q_t/q_e$, Bt could be determined as follows:

$$Bt = -0.4977 - \ln(1 - F), \quad (23)$$

where F and Bt are, respectively, the fraction of solute adsorbed at different times t and a mathematical function of F . The effective diffusion coefficient D_i (cm²/s) is estimated by applying the calculated B values using the following relation [3, 41, 70, 71]:

$$B = \frac{(\pi^2 D_i)}{r^2}, \quad (24)$$

where r is the mean radius of the particle determined by sieve analysis and by assuming them as spherical particles.

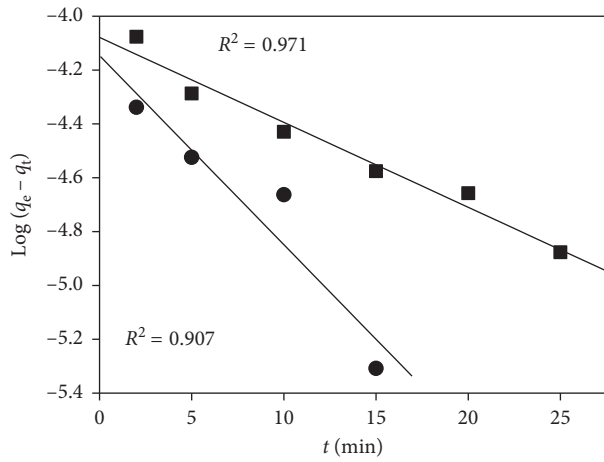
The linear regression graphs of adsorption kinetics for IC and 2,6-DCPIP adsorption onto CTAB-modified POF are shown in Figure 13, and the corresponding constants are summarized in Table 4.

The data in Table 4 indicate that, compared to the pseudo-first-order and Elovich model, the pseudo-

second-order model is perfectly appropriate to describe the adsorption kinetics of IC and 2,6-DCPIP on the CTAB-modified POF with a high correlation coefficient ($R^2 \geq 0.998$). Moreover, it can be observed that the calculated q_e values from pseudo-second-order model are close to the experimental q_e values obtained during the adsorption process at equilibrium, indicating that the adsorption of IC and 2,6-DCPIP onto CTAB-modified POF is a process that is governed by chemisorption [1, 3]. On the other hand, the values of the initial rate of reaction and the reaction half time determined from pseudo-second-order model confirm that the adsorption onto CTAB-modified POF of IC (100.604 $\mu\text{mol}\cdot\text{g}^{-1}\cdot\text{min}^{-1}$; 2.328 min) is faster than 2,6-DCPIP (45.683 $\mu\text{mol}\cdot\text{g}^{-1}\cdot\text{min}^{-1}$; 2.457 min) [3, 58, 72].

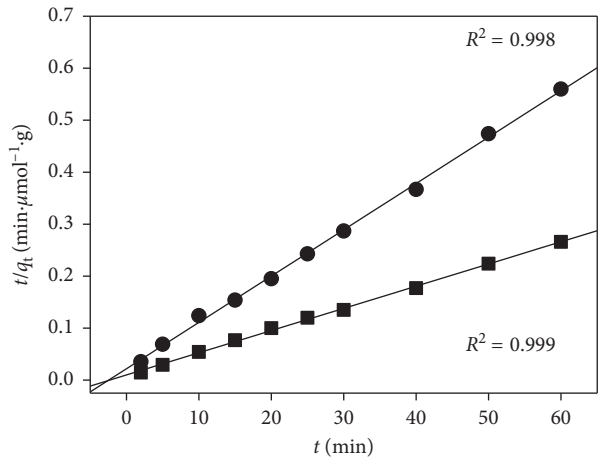
As shown from Figure 13(c), the curves of intraparticle diffusion are equipped with two linear portions for both dyes, which elucidate the two adsorption stages. The first section of plots located at the beginning of the process indicates that boundary layer diffusion or film diffusion probably limited dye adsorption. In this section, the IC and 2,6-DCPIP molecules diffuse through the solution to the external surface of CTAB-modified POF. The second section of plots located at the end of the process indicates intraparticle diffusion or pore diffusion as the adsorption limiting step [3, 73]. Figure 13(c) and Table 4 also show that the first stage is faster than the second one, which may be assigned to the very slow diffusion of the IC and 2,6-DCPIP molecules from the surface film into the micropores in which the adsorption sites are less accessible. The deviation of intraparticle diffusion model curves from the origin of the graph is an indication that IC and 2,6-DCPIP molecules diffusion in the bulk of CTAB-modified POF is not the only rate-controlling step that governs the adsorption [3, 10, 17]. The values of the thickness of boundary layer C for each linear portion are different to zero, meaning that intraparticle diffusion is present in the diffusion process, but it is not the sole rate-controlling step in all the stages [3, 55]. Moreover, the larger C values at the second portion for both dyes, correspond to a greater boundary layer diffusion effect [3, 52]. In addition, a greater C value of IC (217.767 $\mu\text{mol}\cdot\text{g}^{-1}$) compared to a lower C value of 2,6-DCPIP (90.936 $\mu\text{mol}\cdot\text{g}^{-1}$) indicated that IC diffuses more in the interlayer of CTAB-modified POF than 2,6-DCPIP.

Figure 13(e) shows that the Boyd model straight lines deviate from the origin of the graph, signifying that external mass transfer mainly governs the rate controlling step at the initial stages [3, 14, 55, 70]. Table 4 shows that the values of D_i (3.070 $\times 10^{-9}$ cm²/s for IC and 6.843 $\times 10^{-9}$ cm²/s for 2,6-DCPIP) are found between 1×10^{-13} and 1×10^{-5} cm²/s, indicating that chemisorption takes place during the adsorption process [3, 72]. This result corroborates with what was already noted with pseudo-second-order and Dubinin-Radushkevich models. Thus, the adsorption of IC and 2,6-DCPIP on the CTAB-modified POF is best described by external mass transfer diffusion rather than internal diffusion. A similar observation was reported in our previous work [3].



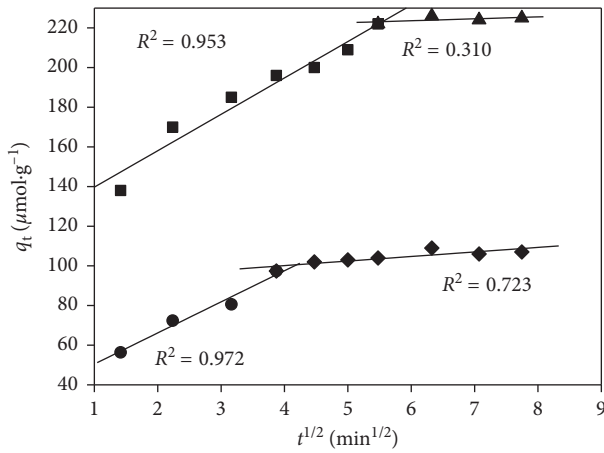
■ IC
● 2,6-DCPIP

(a)



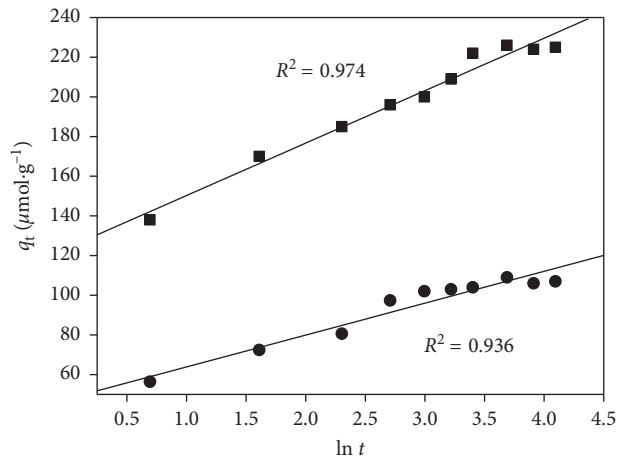
■ IC
● 2,6-DCPIP

(b)



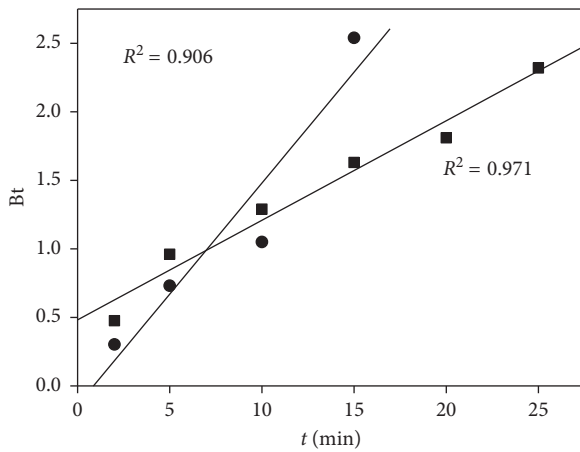
■ IC₁
▲ IC₂
● 2,6-DCPIP₁
◆ 2,6-DCPIP₂

(c)



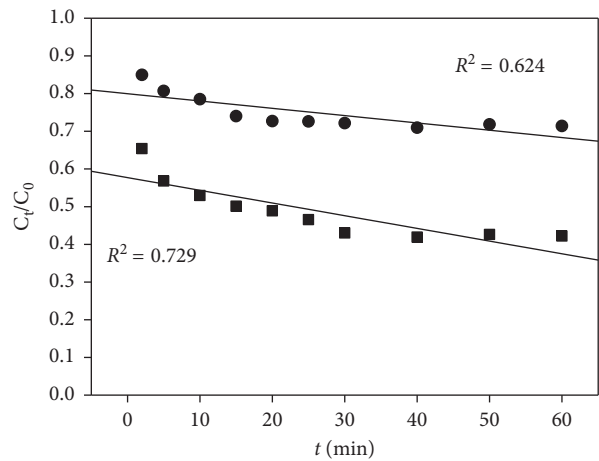
■ IC
● 2,6-DCPIP

(d)



■ IC
● 2,6-DCPIP

(e)



■ IC
● 2,6-DCPIP

(f)

FIGURE 13: Linear regression of adsorption kinetics of (a) pseudo-first-order, (b) pseudo-second-order, (c) intraparticle diffusion, (d) Elovich, (e) Boyd, and (f) external mass transfer.

TABLE 4: Pseudo-first order, pseudo-second-order, Elovich, external mass transfer, Boyd, and intraparticle diffusion parameters for IC and 2,6-DCPIP adsorption onto CTAB-modified POF.

Kinetic models	Constants	IC	2,6-DCPIP
Pseudo-first-order model	q_{exp} ($\mu\text{mol}\cdot\text{g}^{-1}$)	222.107	102.306
	q_e ($\mu\text{mol}\cdot\text{g}^{-1}$)	83.414	71.385
	$K_{1_{ads}}$ (min^{-1})	0.014	0.030
	R^2	0.971	0.907
Pseudo-second-order model	q_{exp} ($\mu\text{mol}\cdot\text{g}^{-1}$)	222.107	102.306
	q_e ($\mu\text{mol}\cdot\text{g}^{-1}$)	234.192	112.233
	$K_{2_{ads}}$ ($\text{g}\cdot\mu\text{mol}^{-1}\cdot\text{min}^{-1}$)	0.002	0.004
	h ($\mu\text{mol}\cdot\text{g}^{-1}\cdot\text{min}^{-1}$)	100.604	45.683
	$t_{1/2}$ (min)	2.328	2.457
	R^2	0.999	0.998
Elovich model	α ($\text{mmol}\cdot\text{g}^{-1}\cdot\text{min}^{-1}$)	2.860	0.315
	β ($\text{g}\cdot\mu\text{mol}^{-1}$)	0.038	0.062
	R^2	0.974	0.936
External mass transfer	$\beta_L S \times 10^3$ (min^{-1})	3.370	1.940
	R^2	0.729	0.624
Boyd model	B (min^{-1})	0.073	0.162
	$D_i \times 10^9$ (cm^2/s)	3.070	6.843
	R^2	0.971	0.906
Intraparticle diffusion model	K_{ip_1} ($\mu\text{mol}\cdot\text{g}^{-1}\cdot\text{min}^{-1/2}$)	18.322	13.739
	K_{ip_2} ($\mu\text{mol}\cdot\text{g}^{-1}\cdot\text{min}^{-1/2}$)	0.974	2.298
	C_1 ($\mu\text{mol}\cdot\text{g}^{-1}$)	121.445	38.601
	C_2 ($\mu\text{mol}\cdot\text{g}^{-1}$)	217.767	90.936
	R_1^2	0.953	0.953
	R_2^2	0.310	0.723

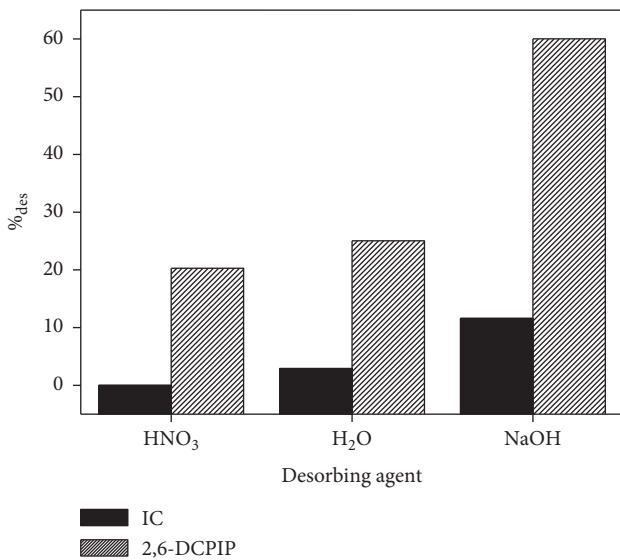


FIGURE 14: Effect of desorption solution on the recovery of IC and 2,6-DCPIP adsorbed. Experimental conditions: 4 mg of IC or 2,6-DCPIP loaded biosorbents; $G = 0\text{--}100\ \mu\text{m}$; $t = 40\ \text{min}$ for IC and $t = 30\ \text{min}$ for 2,6-DCPIP; $v = 150\ \text{rpm}$; $V = 30\ \text{mL}$; at room temperature.

3.10. Desorption. In this study, the desorbing agents as NaOH, HNO₃ ($1 \times 10^{-4}\ \text{mol}\cdot\text{L}^{-1}$), and H₂O were used to regenerate CTAB-modified POF. The results illustrated in Figure 14 show that the higher desorption percentage, 11.58% for IC and 60.03% for 2,6-DCPIP, is obtained in

NaOH solution. This result can be explained by the phenomenon of anionic exchange between the hydroxyl ions (OH⁻) of NaOH solution and the anionic dyes loaded with CTAB-modified POF. The low desorption percentage obtained with IC compared to 2,6-DCPIP is due to the strong bond formed between the IC ions and the CTAB-modified POF [3, 26]. However, the very low desorption percentage of IC represents the fact that the IC molecules and CTAB-modified POF are bound through strong interaction leading to high stability of IC loaded with CTAB-modified POF [2, 19, 44].

4. Conclusions

From this study, the capacity of CTAB-modified POF for the removal of IC and 2,6-DCPIP from aqueous solution has been investigated and the following conclusions can be made. The biosorbent characterizations proved the successful impregnation of CTAB onto raw POF. The new material is an efficient biosorbent for the removal of the two dyes, but the removal of IC showed better performance than that of 2,6-DCPIP. The adsorption performances were strongly affected by various operating parameters such as treatment of biosorbent, contact time, pH of solution, initial concentration of dyes, biosorbents dosage, and ionic strength, even though the ionic strength does not affect the adsorption capacity of 2,6-DCPIP. The nonlinear regressions of adsorption isotherms were investigated, and the values of coefficient of determination and chi-square test showed that Freundlich and Temkin isotherms are most appropriate to describe the adsorption of IC and 2,6-DCPIP on CTAB-

modified POF, respectively. The comparison of the adsorption of IC and 2,6-DCPIP by some adsorbents was shown, and CTAB-modified POF has a significant potential for the adsorption of dyes from an aqueous solution. Results of adsorption kinetics indicated that the adsorption processes were best described by pseudo-second-order kinetics. The diffusion mechanism was studied, and the results showed that external mass transfer was predominant in the rate controlling step. Desorption using NaOH solution as the desorbing agent recovers a maximum quantity of IC and 2,6-DCPIP and considers the reuse of CTAB-modified POF. From the results obtained, the valorization of CTAB-modified POF for the removal of anionic dyes from dye polluted wastewater such as textile effluents is promising.

Data Availability

All data included in our manuscript are available.

Conflicts of Interest

The authors declare that there are no conflicts of interest regarding the publication of this paper.

Acknowledgments

The authors acknowledge the support of the International Foundation for Science (IFS) and the Organisation for the Prohibition of Chemical Weapons (OPCW) (Grant no. W/5859-1 awarded to Evangeline NJANJA). The authors also thank the support of The World Academy of Sciences for a support through the TWAS Research Grants Programme (Project no. 16-515 RG/CHE/AF/AC_G_FR3240293302).

References

- [1] S. Chakraborty, S. Chowdhury, and P. Das Saha, "Adsorption of Crystal Violet from aqueous solution onto NaOH-modified rice husk," *Carbohydrate Polymers*, vol. 86, no. 4, pp. 1533–1541, 2011.
- [2] S. Ibrahim, I. Fatimah, H.-M. Ang, and S. Wang, "Adsorption of anionic dyes in aqueous solution using chemically modified barley straw," *Water Science and Technology*, vol. 62, no. 5, pp. 1177–1182, 2010.
- [3] M. C. D. Ngaha, L. G. Djemmoe, E. Njanja, and I. T. Kenfack, "Biosorption isotherms and kinetics studies for the removal of 2,6-dichlorophenolindophenol using palm tree trunk (*Elaeis guineensis*)," *Journal of Encapsulation and Adsorption Sciences*, vol. 8, no. 3, pp. 156–177, 2018.
- [4] A. A. Jalil, S. Triwahyono, S. H. Adam et al., "Adsorption of methyl orange from aqueous solution onto calcined Lapindo volcanic mud," *Journal of Hazardous Materials*, vol. 181, no. 1–3, pp. 755–762, 2010.
- [5] H. A. Hamad, W. A. Sadik, M. M. Abd El-latif, A. B. Kashyout, and M. Y. Feteha, "Photocatalytic parameters and kinetic study for degradation of dichlorophenol-indophenol (DCPIP) dye using highly active mesoporous TiO₂ nanoparticles," *Journal of Environmental Sciences*, vol. 43, pp. 26–39, 2016.
- [6] V. S. Mane and P. V. Vijay Babu, "Kinetic and equilibrium studies on the removal of Congo red from aqueous solution using Eucalyptus wood (*Eucalyptus globulus*) saw dust," *Journal of the Taiwan Institute of Chemical Engineers*, vol. 44, no. 1, pp. 81–88, 2013.
- [7] A. G. Ulker, E. Mehtap, T. Eliza, and D. Feride, "Mono and simultaneous removal of crystal violet and safranin dyes from aqueous solutions by HDTMA-modified *Spirulina* sp.," *Process Safety and Environmental Protection*, vol. 99, pp. 194–206, 2016.
- [8] M. Greluk and Z. Hubicki, "Comparison of the gel anion exchangers for removal of acid orange 7 from aqueous solution," *Chemical Engineering Journal*, vol. 170, no. 1, pp. 184–193, 2011.
- [9] M. A. Aki, A. M. Youssef, and M. M. Al-Awadhi, "Adsorption of acid dyes onto bentonite and surfactant-modified bentonite," *Journal of Analytical and Bioanalytical Techniques*, vol. 4, no. 4, pp. 1–7, 2013.
- [10] M. Shanker and T. Chinniagounder, "Adsorption of reactive dye using low cost adsorbent: cocoa (*Theobroma cacao*) shell," *World Journal of Applied Environmental Chemistry*, vol. 1, no. 1, pp. 22–29, 2012.
- [11] E. Thiyagarajan, P. Saravanan, S. Shiyamala Devi et al., "Biosorption of reactive red 2 using positively charged *Metapenaeus monoceros* shells," *Journal of Saudi Chemical Society*, vol. 21, no. 1, pp. S1–S6, 2017.
- [12] W. S. Wan Ngah and M. A. K. M. Hanafiah, "Removal of heavy metal ions from wastewater by chemically modified plant wastes as adsorbents: a review," *Bioresource Technology*, vol. 99, no. 10, pp. 3935–3948, 2008.
- [13] M. T. Yagub, T. K. Sen, S. Afroze, and H. M. Ang, "Dye and its removal from aqueous solution by adsorption: a review," *Advances in Colloid and Interface Science*, vol. 209, pp. 172–184, 2014.
- [14] H. Benaïssa and M. A. Elouchdi, "Biosorption of copper (II) ions from synthetic aqueous solutions by drying bed activated sludge," *Journal of Hazardous Materials*, vol. 194, pp. 69–78, 2011.
- [15] R. A. Carletto, C. Fabiana, B. Francesca, and F. Franco, "Adsorption of Congo red dye on hazelnut shells and degradation with *phanerochaete chrysosporium*," *Bioresource*, vol. 3, no. 4, pp. 1146–1155, 2008.
- [16] A. B. Albadarin and C. Mangwandi, "Mechanisms of Alizarin Red S and Methylene blue biosorption onto olive stone by-product: isotherm study in single and binary systems," *Journal of Environmental Management*, vol. 164, pp. 86–93, 2015.
- [17] A. E. A. Said, A. A. M. Alyl, M. M. A. El-Wahab et al., "An efficient biosorption of direct dyes from industrial wastewaters using pretreated sugarcane bagasse," *Energy and Environmental Engineering*, vol. 1, no. 1, pp. 10–16, 2013.
- [18] A. E. Ofomaja and Y.-S. Ho, "Effect of temperatures and pH on methyl violet biosorption by *Mansonia* wood sawdust," *Bioresource Technology*, vol. 99, no. 13, pp. 5411–5417, 2008.
- [19] D. Chen, J. Chen, X. Luan, H. Ji, and Z. Xia, "Characterization of anion-cationic surfactants modified montmorillonite and its application for the removal of methyl orange," *Chemical Engineering Journal*, vol. 171, no. 3, pp. 1150–1158, 2011.
- [20] A. Gladysz-Plaska, M. Majdan, S. Pikus, and D. Sternik, "Simultaneous adsorption of chromium(VI) and phenol on natural red clay modified by HDTMA," *Chemical Engineering Journal*, vol. 179, pp. 140–150, 2012.
- [21] R. Koswojo, R. P. Utomo, Y. Ju et al., "Acid Green 25 removal from wastewater by organo-bentonite from Pacitan," *Applied Clay Science*, vol. 48, no. 1–2, pp. 81–86, 2010.
- [22] M. A. Zenasni, B. Meroufel, A. Merlin, and B. George, "Adsorption of Congo red from aqueous solution using CTAB-kaolin from Bechar Algeria," *Journal of Surface*

- Engineered Materials and Advanced Technology*, vol. 4, no. 6, pp. 332–341, 2014.
- [23] G. L. Dotto, C. Buriol, and L. A. A. Pinto, “Diffusional mass transfer model for the adsorption of food dyes on chitosan films,” *Chemical Engineering Research and Design*, vol. 92, no. 11, pp. 2324–2332, 2014.
- [24] Z. Chen, H. Deng, C. Chen, Y. Yang, and H. Xu, “Biosorption of malachite green from aqueous solutions by *Pleurotus ostreatus* using Taguchi method,” *Journal of Environmental Health Science and Engineering*, vol. 12, no. 63, pp. 1–10, 2014.
- [25] S. Chowdhury and P. Saha, “Sea shell powder as a new adsorbent to remove basic green 4 (malachite green) from aqueous solutions: equilibrium, kinetic and thermodynamic studies,” *Chemical Engineering Journal*, vol. 164, no. 1, pp. 168–177, 2010.
- [26] W. O. W. Maznah, A. T. Al-Fawwaz, and M. Surif, “Biosorption of copper and zinc by immobilised and free algal biomass, and the effects of metal biosorption on the growth and cellular structure of *Chlorella* sp. and *Chlamydomonas* sp. isolated from rivers in Penang, Malaysia,” *Journal of Environmental Sciences*, vol. 24, no. 8, pp. 1386–1393, 2012.
- [27] M. Abbas, S. Kaddour, and M. Trari, “Kinetic and equilibrium studies of cobalt adsorption on apricot stone activated carbon,” *Journal of Industrial and Engineering Chemistry*, vol. 20, no. 3, pp. 745–751, 2014.
- [28] G. Chizari Fard, M. Mirjalili, and F. Najafi, “Hydroxylated α -Fe₂O₃ nanofiber: optimization of synthesis conditions, anionic dyes adsorption kinetic, isotherm and error analysis fiber: optimization of synthesis conditions, anionic dyes adsorption kinetic, isotherm and error analysis,” *Journal of the Taiwan Institute of Chemical Engineers*, vol. 70, pp. 188–199, 2017.
- [29] F. Güzel, H. Saygılı, G. A. Saygılı, and F. Koyuncu, “Decolorisation of aqueous crystal violet solution by a new nanoporous carbon: equilibrium and kinetic approach,” *Journal of Industrial and Engineering Chemistry*, vol. 20, no. 5, pp. 3375–3386, 2014.
- [30] K. C. Nebaghe, Y. El Boundati, K. Ziat, A. Naji, L. Rghioui, and M. Saidi, “Comparison of linear and non-linear method for determination of optimum equilibrium isotherm for adsorption of copper(II) onto treated Martil sand,” *Fluid Phase Equilibria*, vol. 430, pp. 188–194, 2016.
- [31] A. S. Yargıç, R. Z. Y. Sahim, N. Ozbay, and E. Onal, “Assessment of toxic copper(II) biosorption from aqueous solution by chemically-treated tomato waste,” *Journal of Cleaner Production*, vol. 88, pp. 152–159, 2015.
- [32] H. Yazici, M. Kiliç, and M. Solak, “Biosorption of copper(II) by *Marrubium globosum* subsp. *globosum* leaves powder: effect of chemical pretreatment,” *Journal of Hazardous Materials*, vol. 151, no. 2–3, pp. 669–675, 2008.
- [33] G. Kenne Dedzo, C. Péguy Nansou-Njiki, and E. Ngameni, “Amperometric sensors based on sawdust film modified electrodes: application to the electroanalysis of paraquat,” *Talanta*, vol. 99, pp. 478–486, 2012.
- [34] C. B. Njine-Bememba, G. K. Dedzo, C. P. Nansou-Njiki, and E. Ngameni, “Amination of pretreated ayous (*Triplochiton scleroxylon*) sawdust with two organosilanes: characterization, stability, and permselective property,” *Holzforchung*, vol. 69, no. 3, pp. 347–356, 2015.
- [35] A. Adewuyi and F. V. Pereira, “Nitrilotriacetic acid functionalized *Adansonia digitata* biosorbent: preparation, characterization and sorption of Pb (II) and Cu (II) pollutants from aqueous solution,” *Journal of Advanced Research*, vol. 7, no. 6, pp. 947–959, 2016.
- [36] A. Adewuyi and F. V. Pereira, “Preparation and application of EDTA-functionalized underutilized *Adansonia digitata* seed for removal of Cu(II) from aqueous solution,” *Sustainable Environment Research*, vol. 28, no. 3, pp. 111–120, 2018.
- [37] D. L. Postai, C. A. Demarchi, F. Zanatta, D. C. C. Melo, and C. A. Rodrigues, “Adsorption of rhodamine B and methylene blue dyes using waste of seeds of *Aleurites moluccana*, a low cost adsorbent,” *Alexandria Engineering Journal*, vol. 55, no. 2, pp. 1713–1723, 2016.
- [38] H. Saygili and F. Güzel, “High surface area mesoporous activated carbon from tomato processing solid waste by zinc chloride activation: process optimization, characterization and dyes adsorption,” *Journal of Cleaner Production*, vol. 113, pp. 995–1004, 2016.
- [39] M. Calero, A. Pérez, G. Blázquez, A. Ronda, and M. A. Martín-Lara, “Characterization of chemically modified biosorbents from olive tree pruning for the biosorption of leadfied biosorbents from olive tree pruning for the biosorption of lead,” *Ecological Engineering*, vol. 58, pp. 344–354, 2013.
- [40] A. Iddou, M. Hadj Youcef, A. Aziz, and M. S. Ouali, “Biosorptive removal of lead (II) ions from aqueous solutions using *Cystoseira stricta* biomass: study of the surface modification effect,” *Journal of Saudi Chemical Society*, vol. 15, no. 1, pp. 83–88, 2011.
- [41] A. E. Ofomaja and E. B. Naidoo, “Biosorption of copper from aqueous solution by chemically activated pine cone: a kinetic study,” *Chemical Engineering Journal*, vol. 175, no. 1, pp. 260–270, 2011.
- [42] Q. Yanhui, T. Junjiang, W. Shuangfei, and M. Hao, “Amine-functionalized sugarcane bagasse: a renewable catalyst for efficient continuous flow Knoevenagel condensation reaction at room temperature,” *Molecules*, vol. 23, no. 1, pp. 1–13, 2018.
- [43] A. Ronda, M. A. Martín-Lara, M. Calero, and G. Blázquez, “Analysis of the kinetics of lead biosorption using native and chemically treated olive tree pruning,” *Ecological Engineering*, vol. 58, pp. 278–285, 2013.
- [44] S. Ibrahim, H.-M. Ang, and S. Wang, “Removal of emulsified food and mineral oils from wastewater using surfactant modified barley straw,” *Bioresource Technology*, vol. 100, no. 23, pp. 5744–5749, 2009.
- [45] U. A. Guler and M. Sarioglu, “Single and binary biosorption of Cu(II), Ni(II) and methylene blue by raw and pretreated *Spirogyra* sp.: equilibrium and kinetic modeling,” *Journal of Environmental Chemical Engineering*, vol. 1, no. 3, pp. 369–377, 2013.
- [46] U. R. Lakshmi, V. C. Srivastava, I. D. Mall, and D. H. Lataye, “Rice husk ash as an effective adsorbent: evaluation of adsorptive characteristics for Indigo Carmine dye,” *Journal of Environmental Management*, vol. 90, no. 2, pp. 710–720, 2009.
- [47] T. N. Ramesh, D. V. Kirana, A. Ashwini, and T. R. Manasa, “Calcium hydroxide as low cost adsorbent for the effective removal of indigo carmine dye in water,” *Journal of Saudi Chemical Society*, vol. 21, no. 2, pp. 165–171, 2017.
- [48] P. Saha, S. Chowdhury, S. Gupta, and I. Kumar, “Insight into adsorption equilibrium, kinetics and thermodynamics of Malachite Green onto clayey soil of Indian origin,” *Chemical Engineering Journal*, vol. 165, no. 3, pp. 874–882, 2010.
- [49] A. - H. Chen and S. - M. Chen, “Biosorption of azo dyes from aqueous solution by glutaraldehyde-crosslinked chitosans,” *Journal of Hazardous Materials*, vol. 172, no. 2–3, pp. 1111–1121, 2009.
- [50] C. Namasivayam and D. Kavitha, “Removal of Congo red from water by adsorption onto activated carbon prepared

- from coir pith, an agricultural solid waste,” *Dyes and Pigments*, vol. 54, no. 1, pp. 47–58, 2002.
- [51] Y. Aldegs, M. Elbarghouthi, A. Elsheikh, and G. Walker, “Effect of solution pH, ionic strength, and temperature on adsorption behavior of reactive dyes on activated carbon,” *Dyes and Pigments*, vol. 77, no. 1, pp. 16–23, 2008.
- [52] K. Ellass, A. Laachach, A. Alaoui, and M. Azzi, “Removal of methyl violet from aqueous solution using a stevensite-rich clay from Morocco,” *Applied Clay Science*, vol. 54, no. 1, pp. 90–96, 2011.
- [53] S. Sangeetha, C. Piyush, and S. Juhee, “Investigation on biosorption of acidic dye from an aqueous solution by marine bacteria, *Planococcus* sp.,” *International Journal of ChemTech Research*, vol. 6, no. 11, pp. 4755–4763, 2014.
- [54] Y. Xue, H. Hou, and S. Zhu, “Adsorption removal of reactive dyes from aqueous solution by modified basic oxygen furnace slag: isotherm and kinetic study,” *Chemical Engineering Journal*, vol. 147, no. 2-3, pp. 272–279, 2009.
- [55] Z. Wu, H. Zhong, X. Yuan et al., “Adsorptive removal of methylene blue by rhamnolipid-functionalized graphene oxide from wastewater,” *Water Research*, vol. 67, pp. 330–344, 2014.
- [56] Y.-S. Ho, T.-H. Chiang, and Y.-M. Hsueh, “Removal of basic dye from aqueous solution using tree fern as a biosorbent,” *Process Biochemistry*, vol. 40, no. 1, pp. 119–124, 2005.
- [57] A. Moussa and T. Mohamed, “Kinetic, equilibrium and thermodynamic study on the removal of Congo red from aqueous solutions by adsorption onto apricot stone,” *Process Safety and Environmental Protection*, vol. 98, pp. 424–436, 2015.
- [58] L. G. Djemmoe, T. E. Njanja, M. C. Ngaha Deussi, and K. I. Tonle, “Assessment of copper(II) biosorption from aqueous solution by agricultural and industrial residues,” *Comptes Rendus Chimie*, vol. 19, no. 7, pp. 841–849, 2016.
- [59] I. A. Aguayo-Villarreal, L. A. Ramírez-Montoya, V. Hernández-Montoya, A. Bonilla-Petriciolet, M. A. Montes-Morán, and E. M. Ramírez-López, “Sorption mechanism of anionic dyes on pecan nut shells (*Carya illinoensis*) using batch and continuous systems,” *Industrial Crops and Products*, vol. 48, pp. 89–97, 2013.
- [60] F. Geyikçi, “Factorial design analysis for adsorption of Indigo Carmine onto Montmorillonite-Evaluation of the kinetics and equilibrium data,” *Progress in Organic Coatings*, vol. 98, pp. 28–34, 2016.
- [61] E. Gutiérrez-Segura, M. Solache-Ríos, and A. Colín-Cruz, “Sorption of indigo carmine by a Fe-zeolitic tuff and carbonaceous material from pyrolyzed sewage sludge,” *Journal of Hazardous Materials*, vol. 170, no. 2-3, pp. 1227–1235, 2009.
- [62] A. G. S. Prado, J. D. Torres, E. A. Faria, and S. C. L. Dias, “Comparative adsorption studies of indigo carmine dye on chitin and chitosan,” *Journal of Colloid and Interface Science*, vol. 277, no. 1, pp. 43–47, 2004.
- [63] M. A. Ahmed, A. A. brick, and A. A. Mohamed, “An efficient adsorption of indigo carmine dye from aqueous solution on mesoporous Mg/Fe layered double hydroxide nanoparticles prepared by controlled sol-gel route,” *Chemosphere*, vol. 174, pp. 280–288, 2017.
- [64] S. M. De Oliveira Brito, H. M. C. Andrade, L. F. Soares, and R. P. de Azevedo, “Brazil nut shells as a new biosorbent to remove methylene blue and indigo carmine from aqueous solutions,” *Journal of Hazardous Materials*, vol. 174, no. 1-3, pp. 84–92, 2010.
- [65] B. Meroufel, O. Benali, M. Benyahia, Y. Benmoussa, and M. A. Zenasni, “Adsorptive removal of anionic dye from aqueous solutions by Algerian kaolin: characteristics, isotherm, kinetic and thermodynamic studies,” *Journal of Materials and Environmental Science*, vol. 4, no. 3, pp. 482–491, 2013.
- [66] B. H. Hameed and M. I. El-Khaiary, “Malachite green adsorption by rattan sawdust: isotherm, kinetic and mechanism modeling,” *Journal of Hazardous Materials*, vol. 159, no. 2-3, pp. 574–579, 2008.
- [67] K. A. G. Gusmão, L. V. A. Gurgel, T. M. S. Melo, and L. F. Gil, “Application of succinylated sugarcane bagasse as adsorbent to remove methylene blue and gentian violet from aqueous solutions: kinetic and equilibrium studies,” *Dyes and Pigments*, vol. 92, no. 3, pp. 967–974, 2012.
- [68] H. Panda, N. Tiadi, M. Mohanty, and C. R. Mohanty, “Studies on adsorption behavior of an industrial waste for removal of chromium from aqueous solution,” *South African Journal of Chemical Engineering*, vol. 23, pp. 132–138, 2017.
- [69] S. Nethaji and A. Sivasamy, “Adsorptive removal of an acid dye by lignocellulosic waste biomass activated carbon: equilibrium and kinetic studies,” *Chemosphere*, vol. 82, no. 10, pp. 1367–1372, 2011.
- [70] N. Sharma and B. K. Nandi, “Utilization of sugarcane bagasse, an agricultural waste to remove malachite green dye from aqueous solutions,” *Journal of Materials and Environmental Science*, vol. 4, no. 6, pp. 1052–1065, 2013.
- [71] K. S. Bharathi and S. T. Ramesh, “Removal of dyes using agricultural waste as low-cost adsorbents: a review,” *Applied Water Science*, vol. 3, no. 4, pp. 773–790, 2013.
- [72] C. P. Nanseu-Njiki, D. G. Kenne, and E. Ngameni, “Study of removal of paraquat from aqueous solution by biosorption onto Ayous (*triplochiton schleroxylon*) sawdust,” *Journal of Hazardous Materials*, vol. 179, no. 1-3, pp. 63–71, 2010.
- [73] D. A. Fungaro, M. Yamaura, and T. E. M. Carvalho, “Adsorption of anionic dyes from aqueous solution on zeolite from fly ash-iron oxide magnetic nanocomposite,” *Journal of Atomic and Molecular Sciences*, vol. 2, no. 4, pp. 305–316, 2011.

